AD A109033

REPORT DOCUMENTATION PAGE		READ INSTRUCTIONS BEFORE COMPLETING FORM
1. REPORT NUMBER 15605.5-EL	2. GOVT ACCESSION NO. AD-A4 O 1 C 33	3. RECIPIENT'S CATALOG NUMBER
4. TITLE (and Subtitle) Ion Implantation and Laser Processing of III-V Compound Semiconductors with Applications to the Fabrication of Microwave Devices		5. TYPE OF REPORT & PERIOD COVERED Final: 1 Jun 78 - 31 May 81
		6. PERFORMING ORG. REPORT NUMBER
7. AUTHOR(s) James F. Gibbons		8. CONTRACT OR GRANT NUMBER(s) DAAG29 78 G 0119
9. PERFORMING ORGANIZATION NAME AND ADDRESS Stanford University Stanford, CA 94305		10. PROGRAM ELEMENT, PROJECT, TASK AREA & WORK UNIT NUMBERS
11. CONTROLLING OFFICE NAME AND ADDRESS U. S. Army Research Office Post Office Box 12211 Research Triangle Park, NC 27709		12. REPORT DATE Oct 81
		13. NUMBER OF PAGES 42
14. MONITORING AGENCY NAME & ADDRESS(If different from Controlling Office)		15. SECURITY CLASS. (of this report) Unclassified
		15a. DECLASSIFICATION/DOWNGRADING SCHEDULE

16. DISTRIBUTION STATEMENT (of this Report)

Approved for public release; distribution unlimited.

17. DISTRIBUTION STATEMENT (of the abstract entered in Block 20, if different from Report)

NA

18. SUPPLEMENTARY NOTES

The view, opinions, and/or findings contained in this report are those of the author(s) and should not be construed as an official Department of the Army position, policy, or decision, unless so designated by other documentation.

19. KEY WORDS (Continue on reverse side if necessary and identify by block number)

ion implantation	impurities
compound semiconductors	diffusion
microwave devices	gallium arsenides
annealing	laser processing

20. ABSTRACT (Continue on reverse side if necessary and identify by block number)

Research was carried out on laser processing of III-V Compound semiconductors, concentrating on the mechanisms that are responsible for annealing ion implanted dopants in GaAs and on the possibility of obtaining laser-assisted diffusion of dopants. Seven papers describing this work have been written during the period covered by this report. A brief overview of these papers is given. The full papers are attached for detailed presentation of experimental conditions, theoretical calculations and results.
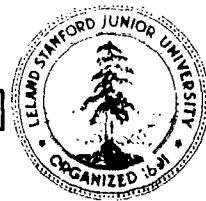
DTIC FILE COPY

DEC 3 0 1981

SOLID STATE ELECTRONICS LABORATORY

STANFORD ELECTRONICS LABORATORIES
DEPARTMENT OF ELECTRICAL ENGINEERING
STANFORD UNIVERSITY · STANFORD, CA 94305

ION IMPLANTATION AND LASER PROCESSING OF III-V COMPOUND SEMICONDUCTORS WITH APPLICATIONS TO THE FABRICATION OF MICROWAVE DEVICES

FINAL REPORT

October 1981

Stanford University
Stanford, CA 94305

Dr. James F. Gibbons
Program Manager and Principal Investigator
Provessor of Electrical Engineering
Stanford Electronics Laboratories

12 30 012

ION IMPLANTATION AND LASER PROCESSING OF III-V COMPOUND

SEMICONDUCTORS WITH APPLICATIONS TO THE FABRICATION OF

MICROWAVE DFVICES

FINAL REPORT

October 1981

Stanford University

Stanford, CA   94305

Dr. James F. Gibbons
Program Manager and Principal Investigator
Professor of Electrical Engineering
Stanford Electronics Laboratories

ION IMPLANTATION AND LASER PROCESSING OF III - V COMPOUND SEMICONDUCTORS

WITH APPLICATION TO THE FABRICATION OF MICROWAVE DEVICES

(Final Report)

Research carried out on laser processing of III - V compound semi-conductors under AROD Contract DAAG29-78-G-0119 concentrated on the mechansims that are responsible for annealing ion implanted dopants in GaAs and on the possibility of obtaining laser-assisted diffusion of dopants. GaAs is a brittle material that decomposes at low temperature. Decomposition (As evaporation) limits the amount of heat that can be transferred to the substrate with a cw laser. Temperature calculations have shown that a beam with an elliptical shape produces a more gradually distributed temperature gradient than a circular beam. It has also been observed that above the threshold of laser induced damage on GaAs, the surface of the wafer decomposes to form the oxide β - Ga_2O_3. Using an elliptical beam, this oxide has been grown continuously by overlapping laser scans with the sample in either laboratory air or an oxygen environment. The heat transferred to the substrate during the growth has allowed the annealing of low dose, deep implanted layers.

Another mechanism that could produce annealing at low substrate temperatures is the epitaxial recrystallization of ion implanted amor-phous layers in the solid phase regime. Complete regrowth in GaAs has been obtained after a thermal anneal at 475°C for 10 minutes, on a sub-strate oriented along the $\langle 511 \rangle$ orientation. A series of As^+ implants, whose doses and energies were selected to achieve a damage density below a critical level, and to insure that its value was maintained in the near surface region, led to complete recrystallization. These implantation conditions represent a set of sufficient conditions lead-ing to solid phase regrowth, but the process is not yet fully control-led. In particular, we have been unsuccessful in attempts to activate dopants implanted within the amorphous layer during the low tempera-ture, short annealing cycle. This process has the potential to enhance cw laser annealing of GaAs at incident laser powers that would leave the substrate free of damage.

FINAL REPORT -- AROD Contract DAAG29-78-G-0119

As a substitute for ion implantation a technique for introducing dopants into GaAs without damaging the substrate has been developed. The source consist of a spin-on SnO_2/SiO_2 film. Tin atoms are diffused into the substrate on active sites by a combination of thermal and laser treatments. A variety of procedures have been studied to explore the possibilities of this technique. Thin n^+ layers on semi insulating GaAs substrates has been obtained this way. In addition to the diffusion, an interface reaction leading to the formation of a tin-arsenide compound (Sn_3As_2) occurs. This structure displays <u>dramatic</u> improvement in ohmic contact properties. Direct evaporation of metal (Al or Ti-Pt-Au) permits the formation of ohmic contacts with low specific contact resistance ($R_{SC} < 1 \times 10^{-6} \ \Omega \ cm^2$). These <u>nonalloyed</u> contacts are found to be thermally stable (up to 400°C) in contrast to conventional Au-Ge contacts. An improvement of the source-drain burn out voltage of gateless MESFETS processed with these contacts has been observed. This contact technology has been then optimized and applied to the fabrication of different GaAs MESFET structures where a single mask can be employed and the same metal used for both the ohmic contacts and the Schottky barrier.

Seven papers describing this work have been written during the period covered by this report. A brief overview of these papers follows this summary. The full papers are attached for detailed presentation of experimental conditions, theoretical calculations and results.

OVERVIEW OF STANFORD PAPERS ON 1 IN IMPLANTATION AND

LASER PROCESSING OF III-V COMPOUND SEMICONDUCTORS

Paper No. 1.

"Temperature Distributions Produced in Semiconductors by a Scanning Elliptical or Circular CW Laser Beam", Y. I. Nissim, A. Lietoila, R. B. Gold, and J. F. Gibbons, Journal of Applied Physics 51, 274, (Jan. 1980).

Contribution: This paper provides a general mathematical solution for the surface temperatures produced by a laser beam scanning over a target having thermal conductivity K(T). Detailed numerical results are presented for silicon and gallium arsenide. The central results of the paper are presented as a set of normalized, "linear temperature" curves. with temperature plotted as a function of (beam power/spot radius). The "true temperature" is obtained from the "linear temperature" for each material by use of a Kirchoff transform. The final results permit specification of experimental conditions to achieve required temperatures.

Paper No. 2.

"CW Laser Annealing of Low Dose Implanted in GaAs", Y. I. Nissim and J. F. Gibbons, in Laser and Electron Beam Solid Interactions and Material Processing, Edited by J. F. Gibbons, L. D. Hess, and T. W. Sigmon (North Holland, New York, 1981) p. 275.

Contribution: This paper demonstrates that higher surface temperatures can be induced in GaAs by using an elliptical scanning beam and letting the surface decompose to form the oxide β-Ga_2O_3. As a consequence of higher induced temperatures, low dose, deep Si implanted layers are annealed.

Paper No 3.

"Solid Phase Epitaxial Regrowth of Ion Implanted Layers in GaAs", Y. I. Nissim, L. A. Christel, T. W. Sigmon, J. F. Gibbons, T. J. Magee, and R. Ormond, to be published in the Applied Physics Letters.

Contribution: This paper presents a set of sufficient ion implantation conditions that results in complete solid phase epitaxial regrowth of the induced amorphous layer. Limiting factors that are responsible for the usually observed incomplete regrowth are identified.

Paper No. 4.

"Thermal Diffusion of Tin in GaAs from a Spin-On SnO_2/SiO_2 Source",
Y. I. Nissim, J. F. Gibbons, C. A. Evans, Jr., V. R. Deline, and J. C.
Norberg, Applied Physics Letters 37, 89, (1980).

Contribution: This letter describes the sample preparation for diffu-
sion to tin from a spin-on SnO_2/SiO_2 source. A variety of thermal
treatments from fast thermal ramping to longer anneals are presented
with the resulting electrical characteristics of the diffused n^+ layers.

Paper No. 5.

"CW Laser Assisted Diffusion and Activation of Tin in GaAs from a SnO_2/SiO_2 Source", Y. I. Nissim, J. F. Gibbons, T. J. Magee, and R. Ormond,
Journal of Applied Physics 52, 227, (1981).

Contribution: This paper shows that following the thermal ramp des-
cribed in Paper No. 4, cw laser scanning can assist further diffusion
and activation of tin introduced during the ramp. A TEM study results
in the identification of a tin-arsenide compound (Sn_3As_2) during the
treatment.

Paper No. 6.

"Nonalloyed Ohmic Contacts to n-GaAs by CW Laser-Assisted Diffusion
from a SnO_2/SiO_2 Source", Y. I. Nissim, J. F. Gibbons, and R. B. Gold,
IEEE Transaction Electron Devices ED-28, 607 (1981).

Contribution: This paper describes the formation of nonalloyed ohmic
contact of low specific contact resistance on the diffused tin doped
layers as a function of incident laser power. The stability of these
contacts at elevated temperatures as compared to conventional Au-Ge
alloyed ohmic contacts is presented.

Paper No. 7.

"CW Laser Assisted Diffusion of Tin in GaAs for Non-Alloyed Ohmic Contacts",
Y. I. Nissim, J. F. Gibbons, R. B. Gold, and D. M. Dobkin, Electrochemical
Society Meeting, Hollywood Florida, (1980).

Contribution: This presentation describes the application of the non-
alloyed ohmic contacts in GaAs MESFET technology.

Paper #1

"Temperature Distributions Produced in Semiconductors by a
Scanning Elliptical or Circular CW Laser Beam."

Paper #2

"CW Laser Annealing of Low Dose Implanted in GaAs."

Paper #3

"Solid Phase Epitaxial Regrowth of Ion Implanted Layers in GaAs."

Paper #4

"Thermal Diffusion of Tin in GaAs from a Spin-On SnO_2/SiO_2 Source."

Paper #5

"CW Laser Assisted Diffusion and Activation of Tin in GaAs from a
SnO_2/SiO_2 Source."

Paper #6

"Nonalloyed Ohmic Contacts to n-GaAs by CW Laser-Assisted Diffusion
from a SnO_2/SiO_2 Source."

Paper #7

"CW Laser Assisted Diffusion of Tin in GaAs for Non-Alloyed Ohmic
Contacts."

Temperature distributions produced in semiconductors by a scanning elliptical or circular cw laser beam

Y. I. Nissim, A. Lietoila, R. B. Gold, and J. F. Gibbons

Stanford Electronics Laboratories, Stanford, California 94305

Temperature profiles induced by a cw laser beam in a semiconductor are calculated. The calculation is done for an elliptical scanning beam and covers a wide range of experimental conditions. (The limiting case of a circular beam is also studied.) This calculation is developed in the particular cases of silicon and gallium arsenide, where the temperature dependence of the thermal conductivity has been taken into consideration. Using a cylindrical lens to produce an elliptical beam with an aspect ratio of 20, a 1-mm-wide area of an ion-implanted silicon wafer was annealed in a single scan. The experimental data are consistent with the extrapolation of solid-phase epitaxial regrowth rates to the calculated laser-induced temperatures.

PACS numbers: 61.80. − x, 44.90. + c

I. INTRODUCTION

Recently, the use of a scanning cw laser to anneal ion-implanted semiconductors has been reported by several authors.[1,2] It has been shown that, in silicon, if the layer is driven amorphous by the implantation, the annealing mechanism is a solid-phase epitaxial regrowth which proceeds at rates comparable to those obtained for conventional thermal annealing.[3] The function of the laser (or electron beam) in this case is simply to heat the implantation-damaged region to a high temperature (~ 1100–1200 °C) so that complete solid-phase regrowth of the entire damaged layer can occur during the dwell time of the laser (typically 1 msec). Because the annealing time is short and the implanted material is never melted in this process, diffusion of the implanted impurity is negligible during the annealing cycle.

To calculate recrystallization rates and a variety of other phenomena related to cw-beam annealing, it is necessary to know accurately the temperature distribution produced by the beam in the material being annealed. A formalism for calculating the temperature distribution produced by an irradiated beam has already been developed for the case of a stationary[4] and moving[5] circular beam, and calculations based on this formalism have been found to agree well with experimental data. However, there are a number of situations in which a ribbon beam with an elliptical rather than a circular cross section would be desirable. Such a beam could be modeled as having an elliptical profile which is narrow in the direction of the scan and large in the direction perpendicular to the scan. Such an intensity distribution can easily be obtained with a cylindrical lens. Moreover, any ratio between large and small axes of the elliptical beam can be achieved by using the correct set of spherical and cylindrical lenses. In view of its potential importance, we have calculated temperature profiles to be expected for beams having an elliptical cross section. In this paper we present these results as an aid to those who wish to explore the use of elliptical laser beams for heating and annealing experiments.

To minimize the amount of data to be presented, and to make the results valid for any kind of material, we present the calculations in two parts. We develop first an expression for the linear temperature rise induced by a moving elliptical beam in a material that is assumed to have constant thermal conductivity. This calculation is based on the formalism proposed by Cline and Anthony. An analytical expression is obtained for the maximum temperature at the center of the moving beam, and a numerical integration is carried out to obtain all the relevant parameter dependences. A different approach, using the formalism developed by Lax,[4] leads to the same maximum temperature rise.

We next present a more refined set of calculations that take into account the temperature dependence of the thermal conductivity. A Kirchoff transform[6,7] is used with experimental data on the thermal conductivity of Si [8] and GaAs [9] to obtain the "true" temperature profiles for these cases.

Finally, as an application of the results, we compare the theory with an experiment in which laser conditions were arranged so that lines of various widths could be annealed in a single pass of a cw Ar laser over an implantation-amorphized layer. The agreement between the theoretical predictions and the experimental data is found to be excellent.

II. SOLUTION TO THE HEAT EQUATION

We assume that the laser beam is elliptical in an (x,y) plane perpendicular to the direction of laser propagation (z). The ratio between the large axis (r_y) and the small axis (r_x) of the ellipse will be an important parameter in our analysis, defined as: $\beta = r_y/r_x$. We assume a Gaussian laser intensity distribution in both directions, $\hat{x}$ and $\hat{y}$:

$$I = I_0 \exp(-x^2/2r_x^2)\exp(-y^2/2r_y^2). \qquad (1)$$

I_0 can be determined as a function of the power absorbed by the material assuming an infinite surface:

$$I_0 = P(1-R)/2\pi r_x r_y, \qquad (2)$$

where P is the total incident power and R is the coefficient of reflection of the irradiated material. Finally, we write the energy absorbed in the solid if the beam is moving with the velocity v in the x direction:

$$Q = \frac{P(1-R)}{2\pi r_x r_y}\exp\left(-\frac{(x-vt)^2}{2r_x^2}-\frac{y^2}{2r_y^2}\right)f(z). \qquad (3)$$

In Eq. (3) $f(z)$ gives the z dependence of the total absorbed energy.

To solve the heat equation, we use a standard Green's function analysis. The source function for the heat equation,[10]

$$\frac{\partial T}{\partial t} - D\vec{\nabla}^2 T = \frac{Q}{C_p},$$ (4)

is

$$G = G\left(\frac{x',y',z',t'}{x,y,z,t}\right)$$
$$= \exp\left(-\frac{[(x-x')^2 + (y-y')^2 + (z-z')^2]}{4D(t-t')}\right)$$
$$\times [4\pi D(t-t')]^{-3/2}.$$ (5)

We define our coordinate axes in the following way: $x = y = z = 0$ will be the center of the beam at the surface of the material, with the x and y axes lying at the surface of the material, pointing along the small and large axes, respectively, of the elliptical beam. The z axis is along the direction of propagation of the laser beam (i.e., perpendicular to the surface of the material).

In the first step we are going to consider a constant thermal conductivity with respect to temperature which will lead to the linear temperature rise.

Making our observation at a time t at a point (x,y,z), the linear temperature rise is as follows:

$$\Theta = \int_{-\infty}^{t} \int_{-\infty}^{\infty} \int_{-\infty}^{\infty} \int_{-\infty}^{\infty} (Q/C_p)(x',y',z',t')$$
$$\times G(x',y',z',t'/x,y,z,t)\, dx'\, dy'\, dz'\, dt'.$$ (6)

The integration over the different variables can be done separately. The integrals over x' and y' are Gaussian tabulated integrals.

To make the integration over z', we need to define the function $f(z)$ which expresses the penetration of laser energy into the material with respect to depth. Since in most cases of interest $\alpha^{-1} \ll r_x, r_y$, we choose $f(z)$ to be a δ function at the surface of the material. To account for the discontinuity at $z = 0$, we have carried out the integration over z' from $-\infty$ to $+\infty$, and then taken twice its value from mirror image considerations.

After carrying out the integration over x, y, z, the linear temperature is the following:

$$\Theta = \frac{2P(1-R)}{C_p \pi^{3/2}} \int_{-\infty}^{t} \frac{1}{\{4D(t-t')[4D(t-t') + 2r_x^2][4D(t-t') + 2r_y^2]\}^{1/2}}$$
$$\times \exp - \left(\frac{(x-vt')^2}{4D(t-t') + 2r_x^2} + \frac{y^2}{4D(t-t') + 2r_y^2} + \frac{z^2}{4D(t-t')}\right) dt'.$$ (7)

In order to simplify the writing of this expression, we introduce the following dimensionless parameters:

$$X = x/r_x; \quad Y = y/r_x; \quad Z = z/r_x; \quad \beta = r_y/r_x;$$

and we define

$$p = [P(1-R)]/r_x, \quad V = vr_x/2D.$$

After the two successive changes of variables, $t'' = -t'$ and $u = (2Dt''/r_x^2)^{1/2}$, the linear temperature at $t = 0$ can be written:

$$\Theta = \frac{p}{C_p D} \frac{1}{\sqrt{2}\pi^{1/2}} \int_0^{\infty} \frac{1}{[(u^2+1)(u^2+\beta^2)]^{1/2}} \exp$$
$$-\frac{1}{2}\left(\frac{(X+Vu^2)^2}{u^2+1} + \frac{Y^2}{u^2+\beta^2} + \frac{Z^2}{u^2}\right) du.$$ (8)

We can now determine, analytically, the maximum linear temperature, obtained at the center of the ellipse $(X = Y = Z = 0)$ for a stationary beam $(V = 0)$. The integration leads to the following result:

$$\Theta_{\max} = \frac{p}{\beta} \frac{1}{C_p D} \frac{1}{\sqrt{2}\pi^{1/2}} K\left(\frac{\beta^2-1}{\beta^2}\right)^{1/2},$$ (9)

where K is the complete elliptical integral of the first kind.

A similar result can be found by considering the elliptical beam as a superposition of circular beams. We can then write the intensity of an elliptical spot in the following way:

$$I_{\text{ellipse}}(x,y) = \int_{-\infty}^{\infty} I_{\text{circular}}(x,y-y')S(y')\, dy'.$$ (10)

We have to find the weighting function $S(y)$ so that the above

intensity distribution gives the correct elliptical intensity written earlier. An identification leads to:

$$S(y) = \left(\frac{1}{2\pi r_x^2(\beta^2-1)}\right)^{1/2} \exp\left(-\frac{y^2}{2r_x^2(\beta^2-1)}\right)$$ (11)

Using now the expression for the linear temperature for a circular beam presented by Lax,[4] and realizing that the same weighting function will distribute the linear temperature, we have

$$\Theta_{\max} = \int_{-\infty}^{\infty} \Theta^{\text{circle}}(y')S(y')\, dy',$$ (12)

which leads to

$$\Theta_{\max} = \frac{P(1-R)}{C_p D r_x \beta \sqrt{2}\pi^{3/2}} K\left(\frac{\beta^2-1}{\beta^2}\right)^{1/2},$$ (13)

or with our p notation:

$$\Theta_{\max} = \frac{p}{\beta} \frac{1}{C_p D} \frac{1}{\sqrt{2}\pi^{3/2}} K\left(\frac{\beta^2-1}{\beta^2}\right)^{1/2},$$ (14)

which is identical to the result of Eq. (9).

This above result can be used to find the maximum temperature for a circular beam by setting $\beta = r_x/r_y = 1$, then

$$\Theta_{\max}^{\text{circle}} = p/C_p D\, 2\sqrt{2\pi}.$$ (15)

The analytical integration has now been carried as far as possible. To analyze the dependence of the actual temperature on beam and substrate parameters, a numerical integration must be performed. To make the results valid for any
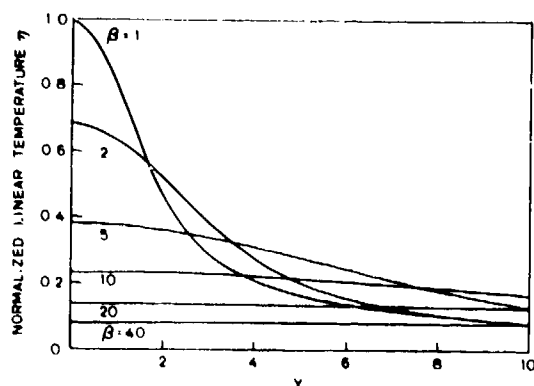
FIG. 1. Linear normalized temperature rise η at $X = Z = V = 0$ as a function of the Y position ($Y = y/r_x$) for different values of β ($\beta = r_y/r_x$) ranging from 1 to 40.

FIG. 3. Linear normalized temperature rise η at $X = Y = V = 0$ as a function of depth Z ($Z = z/r_x$) for different values of β ($\beta = r_y/r_x$) ranging from 1 to 40.

kind of material, we define the following quantity:

$$\eta = \frac{\Theta}{\Theta_{max}^{circle}\,(\beta = 1)} = \frac{2}{\pi} \int_0^\infty \frac{du}{[(u^2 + 1)(u^2 + \beta^2)]^{1/2}}$$
$$\times \exp\left[-\frac{1}{2}\left(\frac{(X + Vu^2)^2}{u^2 + 1} + \frac{Y^2}{u^2 + \beta^2} + \frac{Z^2}{u^2}\right)\right]. \quad (16)$$

III. CALCULATED NORMALIZED LINEAR TEMPERATURE CURVES

The numerical integration of Eq. (16) leads to a set of curves that can be chosen to cover a wide range of experimental conditions. A representative set of such curves is presented here. Figure 1 shows the linearized normal temperature η as a function of the Y ($Y = y/r_x$) position for different values of the ratio β ranging from 1 to 40. We see that large values of β give a more uniform temperature distribution. Under most experimental conditions, we cannot readily decrease r_x, so the only way to obtain high values of β is to increase r_y. A substitution of numbers shows that the power needed to reach an annealing temperature at high values of β
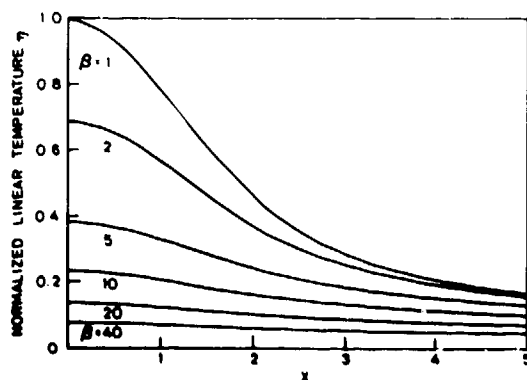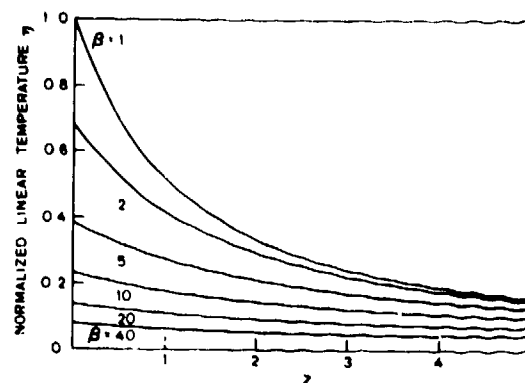
is very high, in fact, above the limit of currently practical cw Ar or Kr lasers, but certainly within the limits of an electron beam.

Similarly, in Figs. 2 and 3, the variations of η in the X ($X = x/r_x$) and Z ($Z = z/r_x$) directions are presented.

An extended scale in the Z direction has been taken in Fig. 4 (for $r_x = 20 \mu m$, the full scale represents $1 \mu m$). This curve shows clearly that the variations near the surface are insignificant and that, for instance, the temperature at the interface of an implanted layer in a semiconductor and underlying substrate is essentially the same as at the surface.

A similar study has been done using beam scanning speed as the parameter for two fixed values of β: $\beta = 1$ and $\beta = 20$. Figures 5 and 6 represent the variation η in the Y direction. Again, in Fig. 6, we can see that if we have enough power for annealing, high speed at $\beta = 20$ gives a uniform temperature distribution along the Y axis. Similarly, Figs. 7 and 8 represent the variations of η in the X direction. Since the beam is moving in this direction the nonsymmetrical behavior with respect to the point $X = 0$ appears clearly in
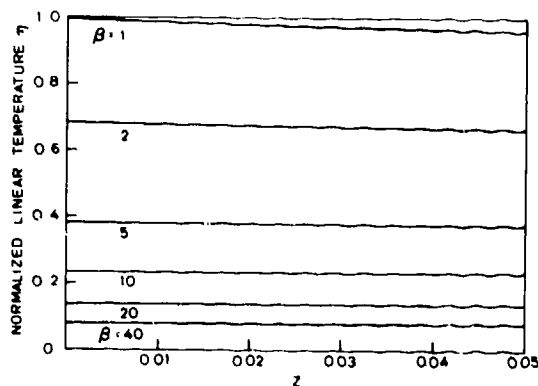

FIG. 2. Linear normalized temperature rise η at $Y = Z = V = 0$ as a function of the X position ($X = x/r_x$) for different values of β ($\beta = r_y/r_x$) ranging from 1 to 40.

FIG. 4. Linear normalized temperature rise η at $X = Y = V = 0$ as a function of depth close to the surface Z ($Z = z/r_x$) for different values of β ($\beta = r_y/r_x$) ranging from 1 to 40.
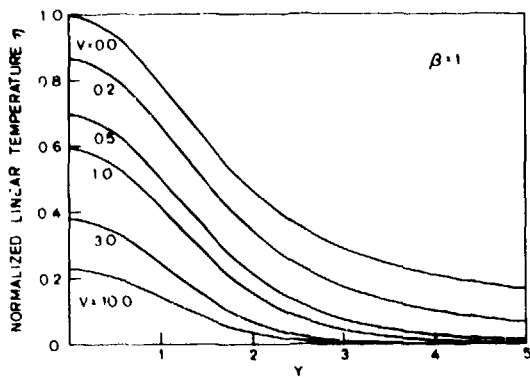
FIG. 5. Linear normalized temperature rise η at $X = Z = 0$ as a function of the Y position ($Y = y/r_s$) for different values of the normalized scan speed V ($V = vr_s/2D$) ranging from 0 to 10 and for $\beta = 1$ ($\beta = r_s/r_s$).
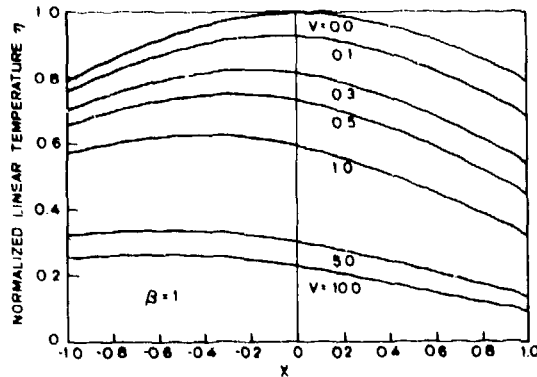

FIG. 7. Linear normalized temperature rise η at $Y = Z = 0$ as a function of the X position ($X = x/r_s$) for different values of the normalized scan speed V ($V = vr_s/2D$) ranging from 0 to 10 and for $\beta = 1$ ($\beta = r_s/r_s$).

these curves. Finally, the variation along Z in Fig. 9 shows again the weak changes of temperature as a function of depth into the material.

In order to allow the reader to use the curves for any combination of speed and ratio β, we have plotted the variation of η as a function of speed with β as a parameter in Figs. 10 and 11. Figure 11 emphasizes the fact that for the typical values of the speed used in a cw laser system, the solid easily reaches thermal equilibrium.

IV. THE TRUE TEMPERATURE RISE IN SILICON AND GALLIUM ARSENIDE

We are now ready to use the Kirchoff transformation[6,7] which leads to the true temperature rise induced by the laser beam. We have chosen to develop these calculations for silicon and gallium arsenide. The temperature-dependent thermal conductivity $K(T)$ has been taken from the literature.

We have been able to fit a rational function to the experimental data by using the form:

$$K(T) = C_p D(T) = A/(T - B). \quad (17)$$

Using this form the relation between the true and linear temperatures is then

$$T = B + (T_{back} - B) \exp\left(\frac{C_p D(T_{back})}{A} \theta\right), \quad (18)$$

where T_{back} is the temperature of the backsurface of the semiconductor.

For silicon we have averaged the experimental data in Ref. 8 to obtain values of: $A = 299$ W/cm and $B = 99$ K. We have verified that a step-by-step numerical integration using published data for $D(T)$ gives a temperature profile which is essentially identical to that obtained using Eq. (17).

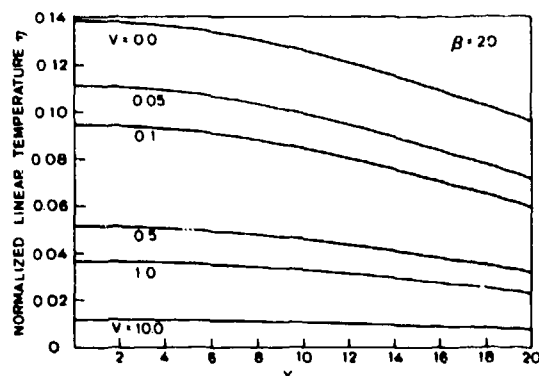For gallium arsenide, we have used experimental data

FIG. 6. Linear normalized temperature rise η at $X = Z = 0$ as a function of the Y position ($Y = y/r_s$) for different values of the normalized scan speed V ($V = vr_s/2D$) ranging from 0 to 10 and for $\beta = 20$ ($\beta = r_s/r_s$).
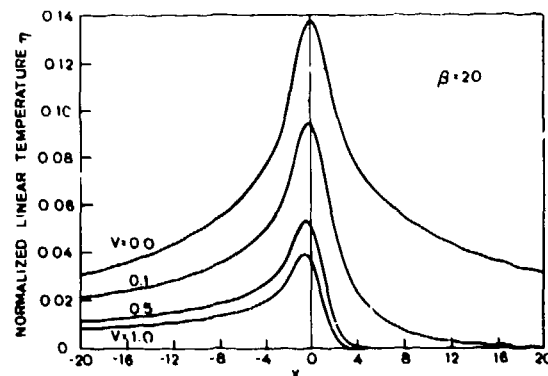

FIG. 8. Linear normalized temperature rise η at $Y = Z = 0$ as a function of the X position ($X = x/r_s$) for different values of the normalized scan speed V ($V = vr_s/2D$) ranging from 0 to 1 and for $\beta = 20$ ($\beta = r_s/r_s$).
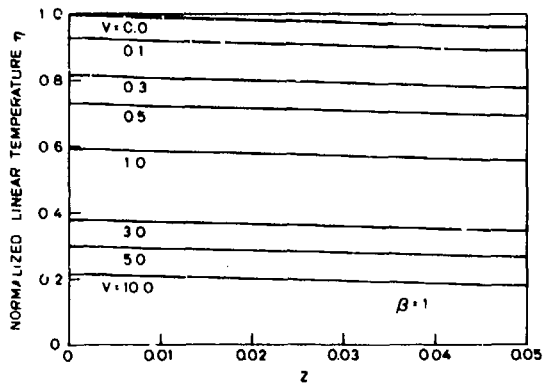
FIG. 9. Linear normalized temperature rise η at $X = Y = 0$ as a function of depth near the surface Z ($Z = z/r_x$) for different values of the normalized scan speed V ($V = vr_x/2D$) ranging from 0 to 10 and for $\beta = 1$ ($\beta = r_y/r_x$).
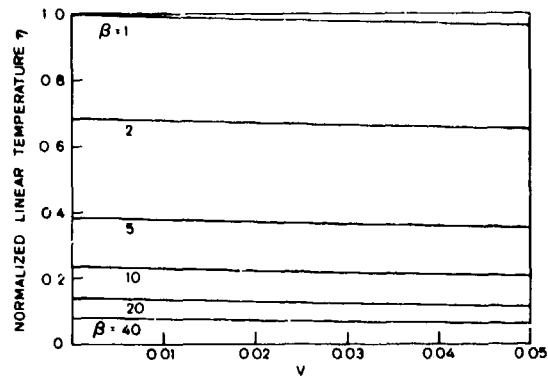

FIG. 11. Extended scale for the linear normalized temperature rise η at $X = Y = Z = 0$ as a function of the normalized scan speed V ($V = vr_x/2D$) for different values of β ($\beta = r_y/r_x$) ranging from 1 to 40.

given by Maycock,[9] which resulted in the following numbers: $A = 91$ W/cm and $B = 91$ K. Since no data are available above $T = 900$ K, we have extrapolated the behavior of $D(T)$ using the same function for higher temperature.

We are now able to obtain the real temperature as a function of p [$p = (1 - R)P/r_x$] for both silicon and gallium arsenide. Figures 12 and 13 present these variations (for $\beta = 1$) for silicon and gallium arsenide, respectively.

V. AN EXPERIMENTAL APPLICATION

The use of an elliptical laser beam to anneal gallium arsenide has already been reported.[11] Such a technique also offers the potential for annealing large areas of ion-implanted silicon in a single scan. Here we have used a 150-mm cylindrical lens to anneal (100) silicon which was arsenic implanted at 100 keV to dose of 6×10^{14} cm^{-2}. The lens employed produces a beam with $r_x = 18$ μm and $\beta = 20$. The annealing parameters were as follows: beam power from 14 to 21 W, back-surface temperature of 550 °C, and scan rate of 1 cm/sec. The reflectivity of the material was measured at room temperature to be $R = 0.38$. Since no melting occurs we will assume R to be constant.

The first annealed area appears at $P = 14.5$ W, which corresponds to a calculated temperature of 967 °C. At $P = 17$ W we can see a line of width $d = 0.4$ mm, as shown in Fig. 14(a). At 21 W of incident power using the same scanning and back-surface temperature setting, we have been able to anneal a 1-mm-wide area, as shown in Fig. 14(b). We can compare these results with those to be expected from the temperature calculations just presented in the following way. First, we assume that the regrowth rate is described by the equation:

$$U = U_0 \exp(- E_a/kT), \tag{19}$$

in which $U_0 = 1.79 \times 10^{15}$ Å/sec and $E_a = 2.35$ eV, as determined by Csepregi and Kennedy.[12]

We have regrown a 1000-Å-thick amorphous layer. The dwell time is approximately $t = 1.7$ msec. The required regrowth temperature is then $T = 977$ °C. Figure 15 shows the temperature profile at the center of the beam ($T = T_{max}$) and at the edge of the beam ($Y = 20$) for our experimental conditions. Knowing that the beam is 1 mm wide we can estimate from this curve the regrown width for temperatures
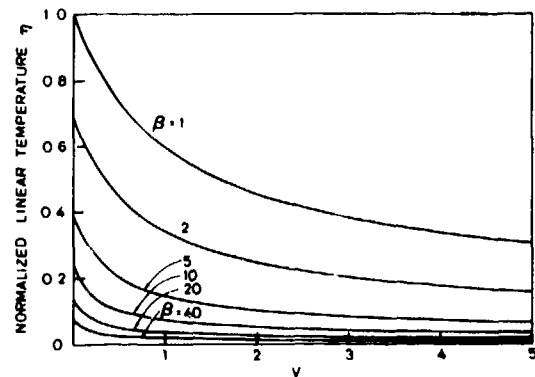

FIG. 10. Linear normalized temperature rise η at $X = Y = Z = 0$ as a function of the normalized scan speed V ($V = vr_x/2D$) for different values of β ($\beta = r_y/r_x$) ranging from 1 to 40.
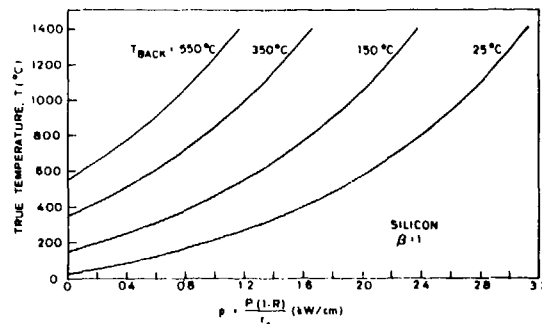

FIG. 12. The true maximum temperature ($X = Y = Z = V = 0$) in Si is plotted versus the normalized power p [$p = [P(1 - R)]/r_x$] for different substrate back-surface temperatures.
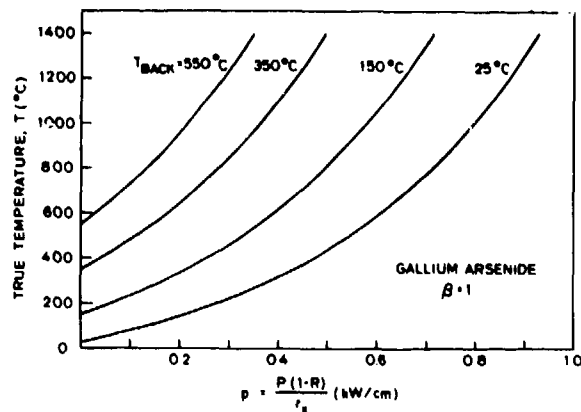
FIG. 13. The true maximum temperature ($X = Y = Z = V = 0$) in GaAs is plotted versus the normalized power p $\{p = [P(1 - R)]/r_x\}$ for different back-surface temperatures.

larger than the calculated one. We can then evaluate that 40% of the beam width has been regrown at 17 W and 100% of the beam width at 21 W. This shows an excellent agreement with our experimental data.

CONCLUSIONS

These calculated results cover a wide range of experimental conditions and can be applied for a laser beam as well
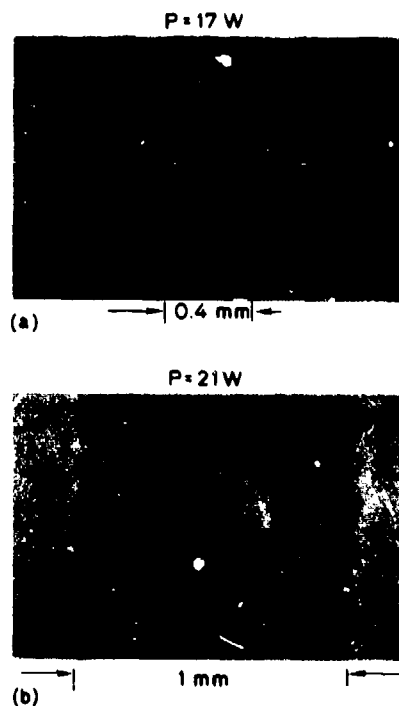

(a)

(b)

FIG. 14. Photomicrographs (55×) of laser-annealed line in silicon using a 150-mm focal length cylindrical lens at (a) $P = 17$ W and (b) $P = 21$ W, $T_{back} = 550$ °C, and $v = 1$ cm/sec. The waviness at the edge of the lines is due to the feedback of the laser working in a light controlled mode.
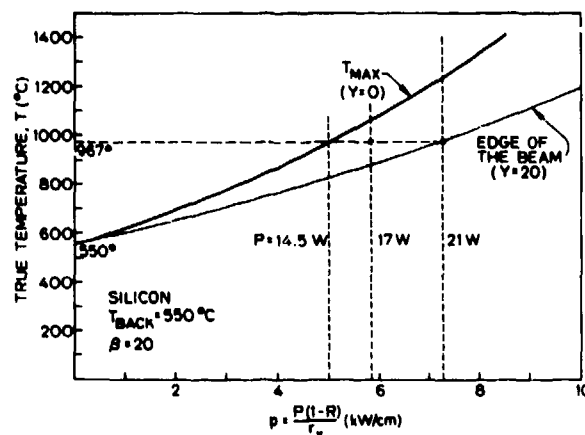

FIG. 15. The true temperature in silicon is plotted at the center of the beam, $Y = 0$, and at the Y edge of the beam, $Y = 20$, for $\beta = 20$ ($\beta = r_y/r_x$). With our experimental conditions, the temperature required for solid-phase epitaxial regrowth is indicated so that the expected width of an annealed line can be determined as a function of laser power. The 17- and 21-W points are shown.

as an electron beam. The calculated linear temperature is valid for any material. With knowledge of the temperature-dependent thermal conductivity, a simple transformation leads to the true temperature. The use of elliptical beam permits large areas to be laser annealed in a single scan. Furthermore, it has the advantage of producing the same annealing as a large radius circular spot will produce but with substantially less laser power.

ACKNOWLEDGMENTS

[1]G.A. Katchurin, E.V. Nidaev, A.V. Khodyachikh, and L.A. Kovaleva, Sov. Phys.–Semicond. 10, 1128 (1976).
[2]A. Gat, J.F. Gibbons, T.J. Magee, J. Peng, V.R. Deline, P. Williams, and C.A. Evans, Jr., Appl. Phys. Lett. 32, 276 (1978).
[3]A. Gat, A. Lietoila, and J.F. Gibbons, J. Appl. Phys. 50, 2926 (1979).
[4]M. Lax, J. Appl. Phys. 48, 3919 (1977).
[5]H.E. Cline and T.R. Anthony, J. Appl. Phys. 48, 3895 (1977).
[6]W.B. Joyce, Solid-State Electron. 18, 321 (1975).
[7]M. Lax, Appl. Phys. Lett. 33, 786 (1978).
[8]C.Y. Ho, R.W. Powell, and P.E. Liley, J. Phys. Chem. Ref. Data 3, Suppl. 1, I-588 (1974).
[9]P.D. Maycock, Solid-State Electron. 10, 161 (1967).
[10]H.S. Carslaw and J.C. Jaeger, Conduction of Heat in Solids, 2nd ed. (Oxford U.P., New York, 1959).
[11]J.C.C. Fan, J.P. Donnelly, C.O. Bozler, and R.L. Chapman, Proc. 7th Int. Symp. On GaAs and Related Compounds, St. Louis, 1978 (Institute of Physics, London, 1979), p. 472.
[12]L. Csepregi and E.F. Kennedy, Proc. of the Symposium on Thin-Film Phenomena Interfaces and Interactions, edited by J.E.E. Baglin and J.M. Poate (Electrochemical Society, Princeton, N.J. 1978), p. 77.

CW LASER ANNEALING OF LOW DOSE IMPLANTS IN GaAs

YVES I. NISSIM AND JAMES F. GIBBONS
Stanford Electronics Laboratories, Stanford, California, 94305

ABSTRACT

The possibility of annealing low dose implants ($\sim 10^{13}$ cm^{-2}) in GaAs using a cw scanning laser has been investigated. We have observed that above the threshold of laser-induced damage, a gallium oxide ($\beta-Ga_2O_3$) can be grown at laser scan speeds of ~ 0.5 mm/sec. The heat transferred to the substrate during the growth of the oxide is utilized to anneal low dose Si implanted layers. As suggested by sheet electrical measurements, close to complete activation of the implanted species is obtained.

INTRODUCTION

A considerable interest has developed during the last four years in the use of lasers and electron beams for processing of Si and GaAs. GaAs, being a much more brittle and unstable material than Si, has enjoyed only moderate success with both pulsed and cw irradiations. Annealing with a pulsed beam has resulted in good activation and recrystallization for high and medium implanted doses [1], although with anomalously low mobilities. Cw laser irradiation has been reported [2] for medium dose implants. Significant activation and high mobilities have been obtained. However, in both techniques, the annealing of low doses (typically used for active channels in GaAs MESFETs) has been largely unsuccessful.

One of the major difficulties associated with transient processing of GaAs is that it decomposes (due to As evaporation) at relatively low temperatures. For cw irradiation, these factors limit the amount of incident power one can use to scan a substrate. Deterioration of the surface (slip lines, thermal etching) have been observed at a maximum induced temperature of about 800°C using a conventional focusing lens. In this paper we describe a technique to induce higher temperatures in the GaAs by growing a surface oxide during the laser scanning. The thermal stress created by high incident laser power is released in the oxide formation.

The approach described in reference [2] using an elliptical beam is employed to anneal low dose (10^{13} cm^{-2}) implants in GaAs. Results below the laser damage threshold are first described, leading to relatively poor annealing. As the incident power is increased, a gallium oxide ($\beta-Ga_2O_3$) is formed at scanning speeds of ~ 0.5 mm/sec. An analysis of the laser parameters that optimize the growth of this oxide over a large area is presented. Auger spectroscopy and x-ray analysis are used to study the composition and identify the oxide. The formation of $\beta-Ga_2O_3$ will provide enough heat to the substrate to anneal deep implanted layers.

PRELIMINARY RESULTS

Cr-doped GaAs substrates oriented along the $\langle 100 \rangle$ direction were used in this experiment. Silicon (SiH^+) ions at a dose of 10^{13} cm^{-2} and an energy of 120 keV were implanted. Co-implants of Si (5×10^{12} cm^{-2} at 120 keV) and S (5×10^{12} cm^{-2} at 140 keV) were also performed in an effort to encourage Si incorporation onto Ga sites. The annealing was carried out using the cw laser apparatus described

in reference [3]. The annealing parameters necessary to obtain electrical activity are found to be relatively different from those for a conventional annealing. The backsurface temperature was held at 550°C during the scanning to reduce the thermal shock created by the laser. The scanning speed was reduced reduced to values between 0.2 and 0.5 mm/sec. The incident beam was focused onto a cylindrical lens resulting in an elliptical spot of aspect ratio 20 (1000x50 μm) at the focal plane. This beam geometry allowed us to cover a large area with each scan and produce a more gradually distributed lateral temperature gradient [4]. The beam was then scanned across the wafer with 150 μm between adjacent scan lines. Electrical activity was measured for incident powers ranging from 4.6 W to 6 W. The lower range of powers resulted in a smooth surface. In the higher power range, slip lines started to appear. Furthermore, the edges of the wafer had to be screened and irregularities on the substrate avoided to prevent the substrate from sudden decomposition (As evaporation). It was observed at powers close to 6 W under these conditions that part of the substrate surface would start to decompose under the moving beam leaving behind it a blue layer.

The best electrical measurements obtained for the two kinds of implants are summarized in Table I. At low power (P = 5 W) it can be seen that the choice of co-implant brought higher activation (22%). At higher power (P = 6W) the substrate is almost completely covered by the blue layer. It can be observed from these data that high activation is obtained at the price of low mobility.

TABLE I
Sheet electrical measurement obtained for different incident powers.
At high power (6 W) oxide formation occurs.

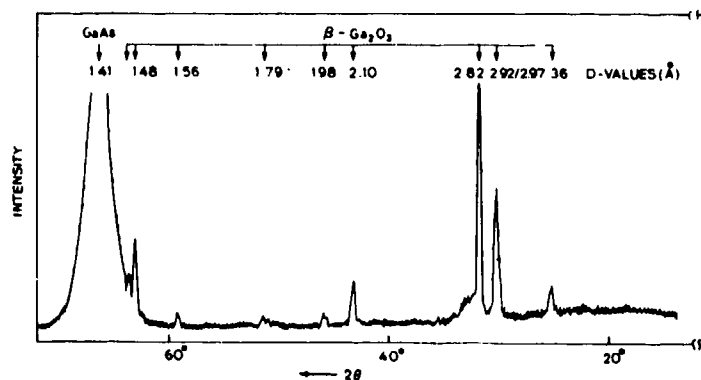|		ρ $\Omega/\square$	μ_H $cm^2/V \cdot sec$	Activation %
Si $\{$ 1 x 10^{13}	P = 5 W	1900	2480	13
120 keV	P = 6 W	3700	460	35
Si $\{$ 5 x 10^{12} + S $\{$ 5 x 10^{12}	P = 5 W	1770	1580	22
120 keV 140 keV	P = 6 W	1650	1480	27

Fig. 1. X-ray spectrum of the oxide layer grown on <100> GaAs. The d values of the peaks correspond to the β-Ga$_2$O$_3$ oxide.

OXIDE FORMATION

The blue surface layer formed with the high power scan has been identified using rotating crystal x-ray analysis to be the gallium oxide γ-Ga_2O_3 shown in Fig. 1. A window of incident laser power and distance between adjacent lines has been determined to form large areas of this oxide. The first observation was that the growth of the oxide occurs at significantly higher incident laser powers than required for annealing. Figure 2(a) shows a micrograph of a single scan obtained at P_a = 6.2 W. By looking at the edge of the line, it is clear that GaAs has been consumed during the formation of γ-Ga_2O_3. A single scan at this power created a 0.5 mm wide oxide strip. Figure 2(b) shows the surface morphology if the same power is used and the lines are scanned with a 150 μm spacing between adjacent scans. Figure 2(c) demonstrates that the morphology can be improved by increasing the power to P_c = 6.8 W. The waviness of the surface indicates that the substrate may have melted during irradiation. Finally, Fig. 2(d) shows an area of the same wafer used in Fig. 2(c) where suddenly at a surface irregularity a thinner oxide (lighter blue) has grown. The overlapping boundaries are barely seen in this portion and the surface structure (waviness) has completely disappeared. In general, good oxides have been grown with powers varying from 5.3 to 6.8 W and step sizes varying from 100 to 250 μm. Many sets of these two parameters were found to form relatively smooth oxides [like Fig. 2(c)], with the general rule that higher powers require higher step size.
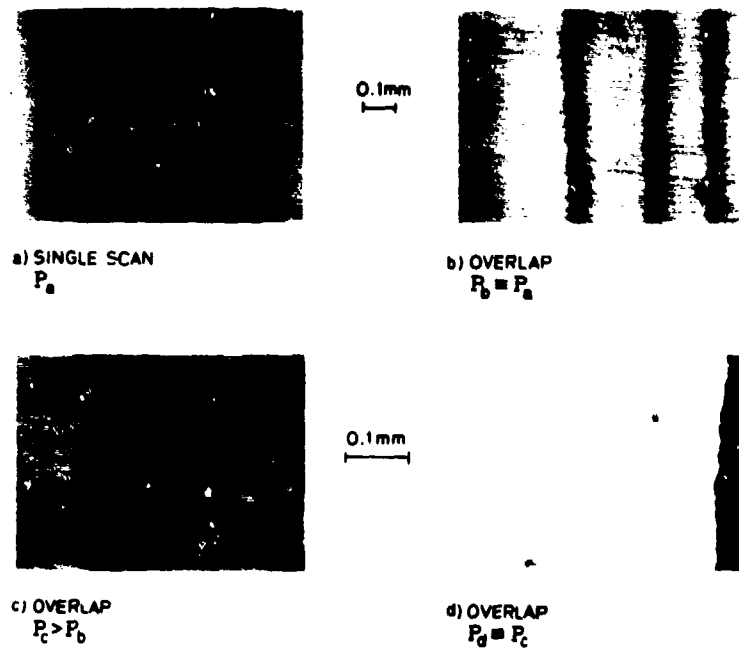

0.1mm

a) SINGLE SCAN
P_a

b) OVERLAP
$P_b = P_a$

0.1mm

c) OVERLAP
$P_c > P_b$

d) OVERLAP
$P_d = P_c$

Fig. 2. Optical micrograph of the laser grown oxide for different incident powers.

The calculation described in refererce [4], was carried out to obtain the maximum temperature and the temperature at the edge of the beam with the results shown in Fig. 3. The distribution of temperatures induced by the laser within the scanning ellipse is then obtained. The working areas for annealing and oxide growth are represented. The overlap between the two areas indicates that the oxide can grow at low powers if the growth is initiated by scanning an edge of the substrate or by making the first laser scan at higher power. While scanning over an already grown layer, the oxide growth will continue.
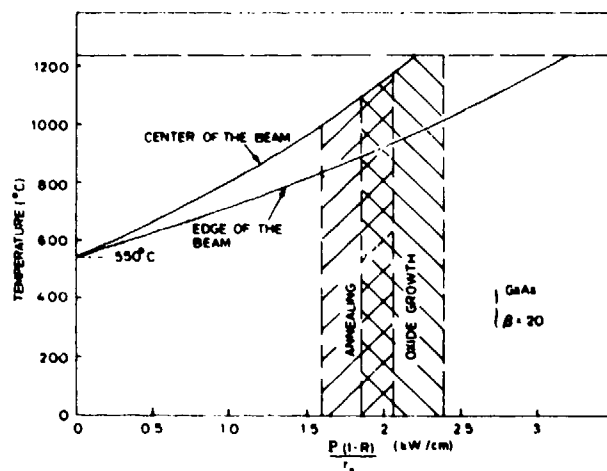

Fig. 3. Temperature induced by the laser on GaAs for a cylindrical lens of aspect ratio 20. The maximum temperature at the center of the beam and the temperature at the edge of the beam are shown.

Sputtering Auger profiling has been used to study the composition of this oxide and its interface with the GaAs substrate. The r ulting profile is shown in Fig. 4. It can be seen that the gallium oxide is completely free of As (within the sensitivity of the measurements) and is about 1200 Å thick (corresponding to the blue color). The interface appears to be relatively thin ($\leq$ 100 Å).

The importance of the ambient during the oxide formation has also been investigated. The laser annealing parameters were kept constant, while a wafer was scanned in three different environments: forming gas (10% H_2, 90% N_2), air, and oxygen. In the first case a grey powder characteristic of a Ga excess, due to As evaporation, is observed. In the second and third environments, a similar blue oxide is obtained, indicating that the reaction is limited by the rate of As evaporation.

Some properties of this oxide have been investigated. It has been observed that it was attacked very slowly by normal acids; 15 min. in boiling HCl was required to remove it. A temperature resistance test showed that the laser grown β-Ga_2O_3 can withstand temperatures as high as 800°C.
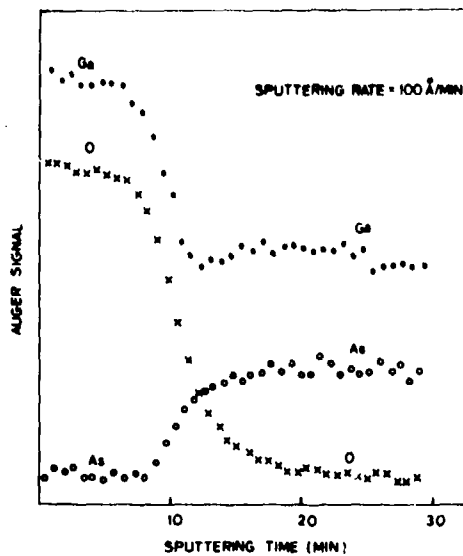
Fig. 4. Sputtering Auger profile of the laser grown oxide.

ANNEALING OF DEEP IMPLANTED LAYERS

The curves of Fig. 3 indicate clearly that higher temperatures can be reached if the sample is allowed to decompose at the surface and form an oxide. Temperatures in the range 1050°C up to the melting point of GaAs can be induced in the substrate. Table I also demonstrates that higher incident powers result in higher dopant activation.

For the Si implantation presented earlier (10^{13} cm^{-2}/120 keV), all the atoms lie within 2600 Å of the surface. After the first 1200 Å are consumed during the growth of the β-Ga$_2$O$_3$, only 37% of the implanted dopants remain. The values obtained in Table I for P = 6 W suggest then that most of the remaining impurity atoms are activated onto substitutional Ga sites. In view of this observation, deeper Si implants have been carried out. A dose of 1×10^{13} cm^{-2} at an energy of 300 keV will leave the first 1200 Å relatively free of implanted atoms. A wafer implanted under these conditions was then annealed while trying to obtain a uniform oxide layer. The oxide layer was then removed in boiling HCl and surface electrical measurements were carried out using a van der Pauw technique. Complete activation of the implanted dopants was measured. The reproducibility from scan to scan has been found to depend on the quality and uniformity of the oxide layer grown. For example, sheet electrical measurements made on the wafers, presented in Figs. 2(b) and 2(c), displayed high carrier concentrations, but the mobility in the case of Fig. 2(b) was significantly lower than for the Fig. 2(c) wafer. The implanted layer beneath the oxide shown in Fig. 2(d) did not show any electrical activity probably because not enough heat was transferred to the substrate during the growth of this thinner layer. The best measurements were obtained for P = 5.8 W and step size of 120 μm. The following values were obtained: sheet resistivity: 350 Ω/□ ; Hall mobility: 1780 cm^2/V·sec; and sheet carrier concentration: 1.01×10^{13} cm^{-2}.

CONCLUSION

It has been shown that a gallium oxide β-Ga_2O_3 can be grown at laser scan speeds of about 0.5 mm/sec on a GaAs substrate. This oxide appears free of As and is both acid and temperature resistant. The stress induced by the laser in GaAs can be released by letting the substrate decompose at the surface and form β-Ga_2O_3. This oxide growth permits significantly higher temperatures to be developed in the GaAs by laser scanning, resulting in the ability to anneal low dose Si implants. The electrical activity as judged by sheet resistance measurements is close to 100% when the impurity content in the oxide film is subtracted.

REFERENCES

1. See for example, F. H. Eisen in: Laser and Electron Beam Processing of Materials, C. W. White and P. S. Peercy eds. (Academic Press, New York 1980) p. 309.

2. J. C. C. Fan, J. P. Donnelly, C. O. Bozler and R. L. Chapman, Proc. 7th International Symposium on GaAs and Related Compounds, 1978 (Institute of Physics, London 1979) p. 47).

3. A. Gat and J. F. Gibbons, Appl. Phys. Lett. 32, 142 (1978).

4. Y. I. Nissim, A. Lietoila, R. B. Gold and J. F. Gibbons, J. Appl. Phys. 51, 274 (1980).

SOLID PHASE EPITAXIAL REGROWTH OF ION IMPLANTED LAYERS IN GaAs

Y. I. Nissim, L. A. Christel, T. W. Sigmon and J. F. Gibbons
Stanford Electronics Laboratories
Stanford, CA 94305

T. J. Magee and R. Ormond
Advanced Research and Application Corporation
Sunnyvale, CA 94086

ABSTRACT

The complete solid phase epitaxial regrowth of ion implanted layers in GaAs was obtained during a short (10 min) capless furnace anneal at a temperature of 475°C. Two factors believed responsible for the incomplete regrowth of layers have been identified. First, the damage density from the implant should not exceed a critical value determined by a Boltzmann calculation. Second, the growth of polycrystalline material from the surface observed by transmission electron microscopy is a competitive mechanism. As$^+$ implants, whose doses and energies were selected to achieve the correct damage density, and to insure that its value was maintained in the near surface region, led to a complete recrystallization.

The annealing of ion implanted GaAs usually requires a thermal treatment at temperatures higher than 600°C. This process is typically carried out in an As overpressure or with an encapsulant to avoid surface decomposition. Recently it has been shown [1] that under certain ion implantation conditions, solid phase epitaxial regrowth of amorphized layers can occur at temperatures of 180°C or above. The dose dependent recrystallization behavior observed in this work can be tentatively explained [2] by the local stoichiometric imbalance resulting from the implantation. More recently, the epitaxial regrowth of thin amorphous films [3] (thickness <400 Å) has been observed. In this work, we have identified some of the factors that appear to be responsible for incomplete regrowth, and have found a set of implantation conditions that will create amorphous layers that can regrow completely using low temperature furnace anneals. These factors are in agreement with the experimental data presented in the studies mentioned above.

The multiple parameter dependence of epitaxial regrowth in Si [4] suggests a large number of experimental conditions that can be studied in GaAs. Based on physical arguments to be described here, a number of experimental choices were made which allowed us to observe the dependence of the regrowth properties on a limited number of parameters. The work reported in Ref. [1] shows that a very fast regrowth rate along the <100> direction exists. In an attempt to control the process, we have chosen to use GaAs oriented along the <511> direction (slower growth direction). The implantations were carried out with the substrate held either at ice water (for the highest dose) or liquid nitrogen temperature, to obtain a sharp crystalline-amorphous interface and reduce the necessary incident dose of amorphization. The contribution of dopant atoms to the regrowth rate is minimized by the implantation of As^+ ions.

- 2 -

Preliminary experiments were performed to determine the time-temperature cycles for the annealing of a truly amorphous layer. A dose of 8×10^{15} As$^+$/cm^2 was implanted at 180 keV into a <511> substrate held at ice water temperature. The analysis of the layer was carried out using 2.2 MeV He$^+$ ion channeling. The channeling measurements showed the existence of a 1400 A thick amorphous surface layer on the as-implanted sample. The wafer was then scribed into several pieces and thermally annealed in flowing nitrogen with different time-temperature cycles to investigate the solid phase epitaxial regrowth. The range of temperatures used was 400° to 500°C in steps of 25°C. For temperatures between 400°C and 475°C, epitaxial growth from the crystalline-amorphous interface was initially observed, but was found to terminate before reaching the surface (40% of the initial amorphous layer consistently recrystallized). At an annealing temperature of 500°C a slow annealing of defects is superimposed to the epitaxial growth. As shown in Fig. 1 this is characterized by a reduction of the backscattering yield with increase in the annealing time without evolution of the damaged layer.

The depth at which the epitaxial growth stops in the preceding experiments is close to the projected range of the As$^+$ ions. The high disturbance of the lattice at this point might then be a factor contributing to the incomplete regrowth. To investigate this effect, samples where prepared with lower incident doses. Implantations of 2×10^{15} As$^+$/cm^2 and 5×10^{13} As$^+$/cm^2 at 145 keV were carried out into <511> substrates held near liquid nitrogen temperature. Figure 2 shows the channeling measurements obtained from as-implanted and annealed samples of the 2×10^{15} As$^+$/cm^2 implant. The as-implanted spectrum displays a 1000 Å thick amorphous layer. After a thermal annealing at 425°C for 10 min, it can be seen that 40% of the amorphous layer thickness

- 3 -

regrew epitaxially from the interface toward the surface and stopped. Anneal-ing at the same temperature for an additional 10 min. produces no change in the backscattering spectrum. The recrystallized region has a high concentra-tion of defects revealed by the high backscattering yield obtained. Similar results were obtained when the incident dose was $8x10^{15}$ As$^+$/cm^2. For the second implant ($5x10^{13}$ As$^+$/cm^2), the damaged layer is not completely amorphous (65% of the random yield) but complete recrystallization is observed after 10 min at 475°C.

In order to investigate the atomic profile in detail, damage distribu-tion and net stoichiometric imbalance resulting from the implantation, a Boltzmann transport calculation was carried out [5,6]. The results of this calculation assuming that incident ions with energy more than 5 keV will create, during the collision with lattice atoms, recoils contributing to the stoichiometric imbalance, are shown in Fig. 3 for the $2x10^{15}$ As/cm^2, 145 keV implant. The interesting results are the minimum damage density required to obtain an amorphous state, $4.8x10^{24}$ eV/cm^3; and the damage density at which the regrowth stopped, $15.6x10^{24}$ eV/cm^3. This upper limit is not yet well established since the recrystallized region is still highly damaged. These results indicate that epitaxial regrowth of GaAs can occur following an implantation that produces a damage density slightly above $4.8x10^{24}$ eV/cm^3.

When driven amorphous, GaAs undergoes a change of reflection coefficient induced by the lattice disorder. This is characterized by a milky appearance compared to the shiny color of the single crystal. For all the previous experiments, the substrate was observed to recover its single crystal color after annealing. This observation indicates that a partial reordering of the lattice at the near surface is taking place. This could be a competitive

regrowth mechanism proceeding from the surface toward the crystal/amorphous layer interface. A multiple implant, leading to a flat dopant concentration profile and damage density would suppress this partial reordering.

Using the above observations a new implantation series was designed. With the substrate held near liquid nitrogen temperature, the following multiple As implantation was performed: $5x10^{14}/cm^2$ at 145 keV followed by $1.7x10^{14}/cm^2$ at 80 keV. This results in a relatively flat damage density profile at a value of $\gtrsim 5x10^{24}$ eV/cm^3. Channeling experiments show the formation of a 800Å thick amorphous layer. As seen in Fig. 4 complete solid phase epitaxial regrowth is obtained after a thermal annealing at 475°C for 10 min. The annealed spectrum shows complete recovery of crystallinity.

The nature of microstructure in the as-implanted and annealed samples for the above cases were studied by standard Transmission Electron Microscopy (TEM) analysis. Figure 5 shows representative bright field electron micrographs obtained from samples amorphized with the multiple implant, before (as implanted) and after annealing at 475°C for 10 min. After implantation, we observe an absence of any resolvable microstructure and the presence of an amorphous layer. This can be seen from the diffraction pattern (inset of Fig. 5[a]). After annealing, complete recrystallization of the amorphous layer is observed and well defined single crystal diffraction patterns are detected. Within the implanted region, residual damage is observed in the form of dislocation loops of 150 to 250 A average diameter [Fig. 5(b)] at concentrations of $\approx 10^{11}/cm^2$.

In contrast, after implantation at the higher dose ($8x10^{15}$ As/cm^2 at 180 keV) and subsequent annealing in the same condition (475°C for 10 min) a substantially different pattern of recovery from the amorphous state is observed. The presence of an amorphous layer after implantation is observed.

After annealing, polycrystallites of GaAs are detected within the implanted region as shown in Fig. 6(a). The ring structure in the diffraction pattern inset confirms the polycrystalline nature of the layer. Careful examination also indicated the possible existence of residual dislocation line structure beneath the polycrystalline layer. Using controlled chemical stripping, 750Å of material was etched from the surface of the sample and specimens were again prepared for TEM examination. Figure 6(b) shows that all the poly-crystalline layer has been removed, and a complex array of dislocation nesting is observed. The diffraction pattern indicates an absence of polycrystalline rings and the presence of an imperfectly regrown single crystal layer at a depth of ∼ 750 Å.

These TEM observations are in excellent agreement with the channeling spectra observed for these implant and anneal conditions. From these results we have obtained the following set of sufficient conditions:

1. The damage density induced by the implantation must be below a critical threshold but above the level of amorphization. Such windows can eventually be found by holding the substrate at 77°K during the implantation.

2. Polycrystalline growth from the surface must be suppressed with a multiple implantation cycle.

The same implantation and anneal cycle was performed on <100> GaAs lead-ing again to a complete lattice recovery. Further work on the <100> orienta-tion and on the electrical activation of dopants during this process for both <511> and <100> orientation is being conducted and will be reported later.

ACKNOWLEDGMENT

REFERENCES

[1] J. S. Williams and M. W. Austin, Appl. Phys. Lett. 36, 994 (1980).

[2] K. Gamo, T. Ineda, J. W. Mayer, F. H. Eisen and C. G. Rhodes, Radiat. Eff. 33, 85 (1977).

[3] M. G. Grimaldi, B. M. Pane, M. Maenpaa, M.-A. Nicolet and D. K. Sadana, unpublished.

[4] L. Csepregi, E. F. Kennedy, J. W. Mayer and T. W. Sigmon, J. Appl. Phys. 49, 3906 (1978).

[5] L. A. Christel, J. F. Gibbons and S. Mylroie, J. Appl. Phys. 51, 6176 (1980).

[6] L. A. Christel and J. F. Gibbons to be published in J. Appl. Phys. (Manuscript R-1309).

FIGURE CAPTIONS

Fig. 1   Channeling spectra illustrating the isothermal annealing behavior at 500°C for 8×10^{15} As^+/cm^2, 180 keV implant into <511> GaAs.

Fig. 2   Channeling spectra illustrating the incomplete epitaxial regrowth at 425°C for 2×10^{15} As^+/cm^2, 145 keV implanted into <511> GaAs.

Fig. 3   Net stoichiometric imbalance and damage distribution in GaAs produced by an implantation of 2×10^{15} As^+/cm^2 at 145 keV (calculation).

Fig. 4   Channeling spectra illustrating the complete epitaxial regrowth at 475°C for 5×10^{14} As^+/cm^2, 145 keV plus 1.7×10^{14} As^+/cm^2, 80 keV implant into <511> GaAs.

Fig. 5   Representative bright field transmission electron micrographs obtained from samples implanted with 145 keV As ions to a dose of 5×10^{14} cm^{-2} plus 80 keV As ions to a dose of 1.7×10^{14} cm^{-2}. (a) As implanted; (b) implanted and annealed at 475°C for 10 min. selected area diffraction patterns characteristic of regions are shown in insets.

Fig. 6   Representative bright field transmission electron micrographs obtained from sample implanted with 180 keV As ions to a dose of 8×10^{15} cm^{-2}. (a) implanted and annealed at 475°C for 10 min. (b) implanted and annealed when 750 Å are stripped from the surface. Insets show selected area diffraction patterns from regions.
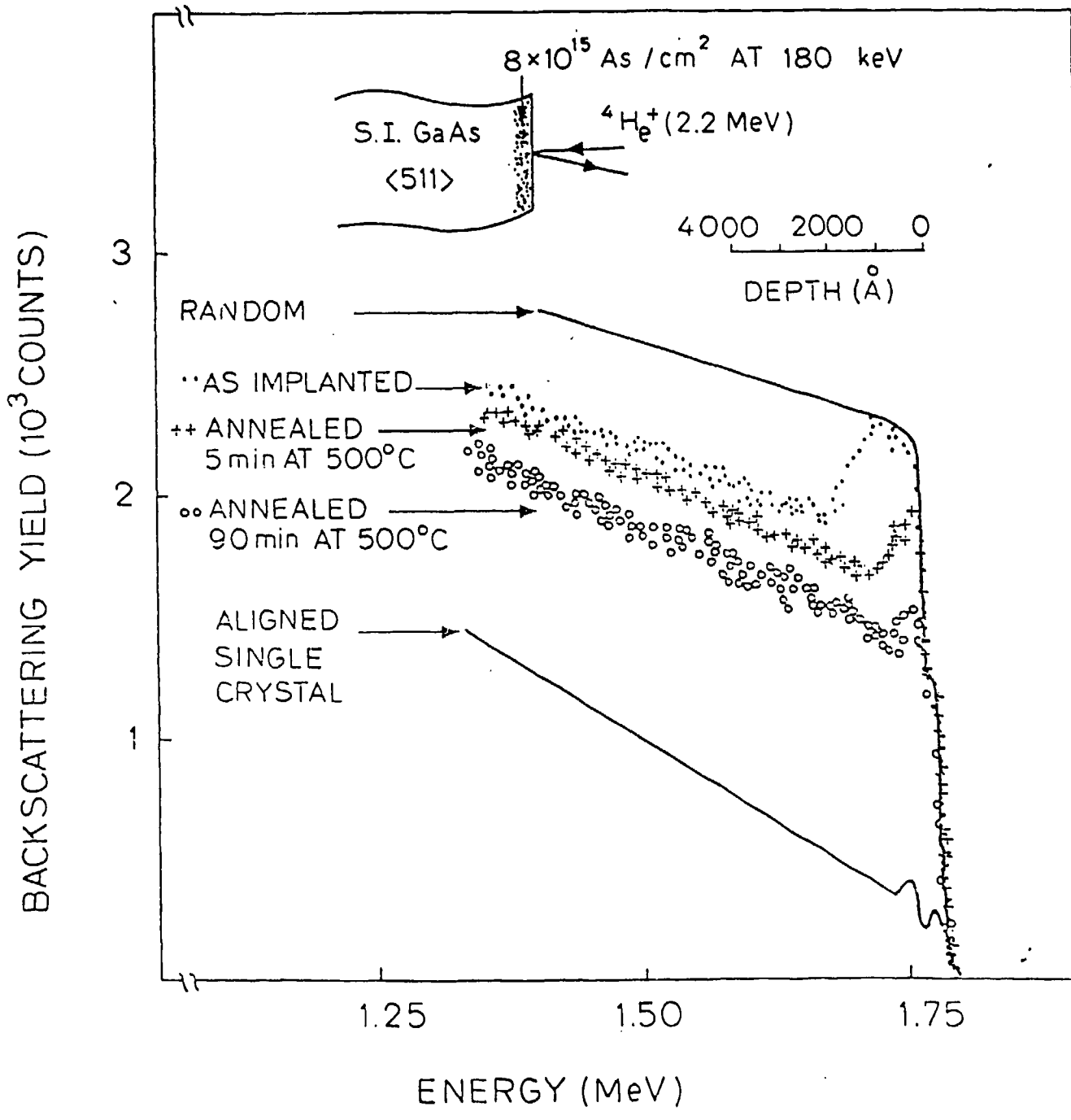
Fig. 1

BACKSCATTERING YIELD (10^3 COUNTS)

8×10^{15} As /cm^2 AT 180 keV

S.I. GaAs
⟨511⟩

$^4He^+$ (2.2 MeV)

4000 2000 0
DEPTH (Å)

RANDOM

·· AS IMPLANTED
++ ANNEALED
5 min AT 500°C
∘∘ ANNEALED
90 min AT 500°C

ALIGNED
SINGLE
CRYSTAL

1.25   1.50   1.75

ENERGY (MeV)

Fig 2

Fig 3

Fig 4

5×10^{14} As/cm^2 AT 145 keV
+1.7×10^{14} As/cm^2 AT 80 keV

S.I. GaAs ⟨511⟩

$^4H_e^+$ (2.2 MeV)

2000   0

DEPTH (Å)

RANDOM

AS IMPLANTED

°° ANNEALED
10 MIN AT 475°C

ALIGNED
SINGLE CRYSTAL

BACKSCATTERING YIELD (10^5 COUNTS)

3

2

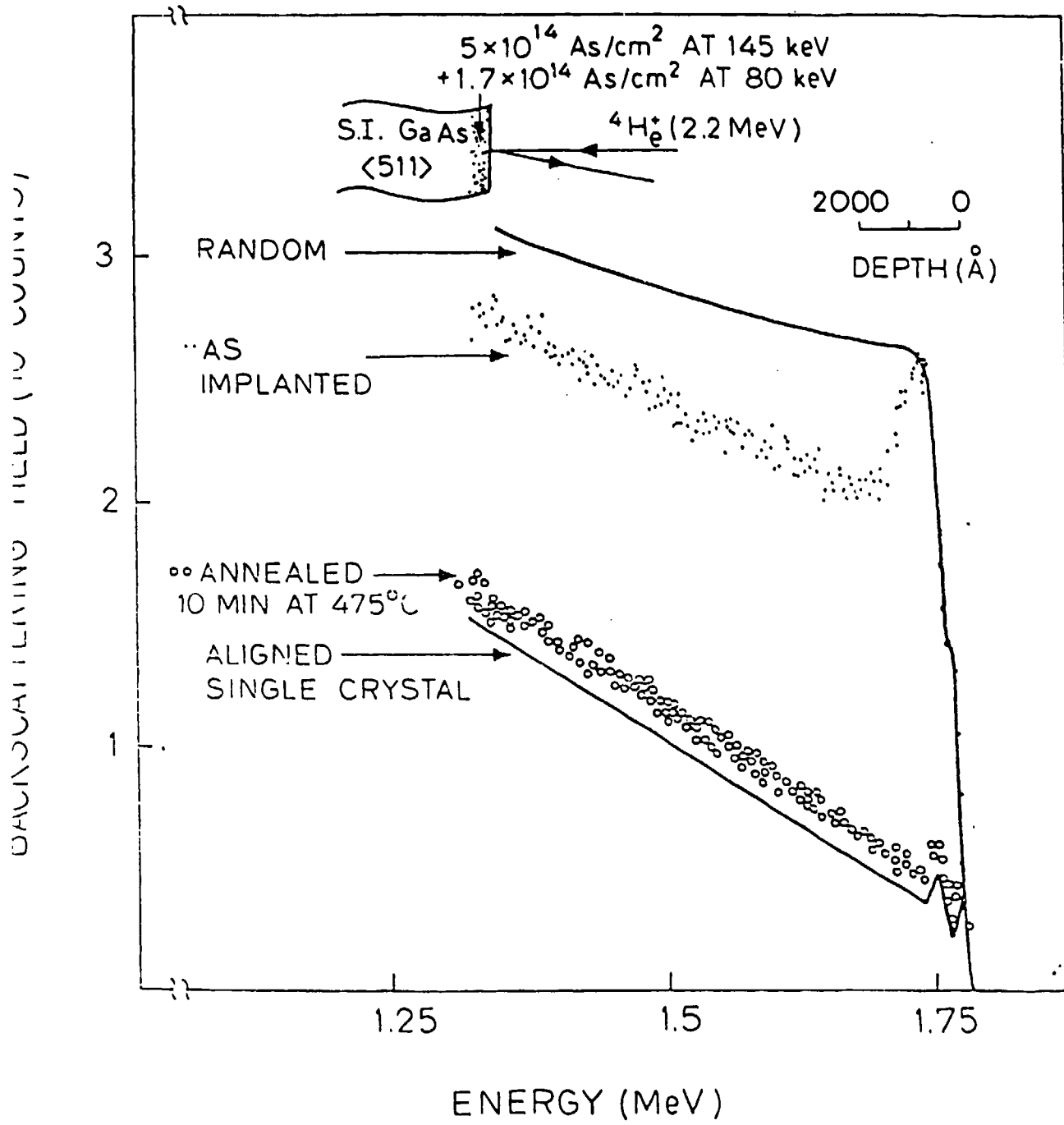1

1.25   1.5   1.75
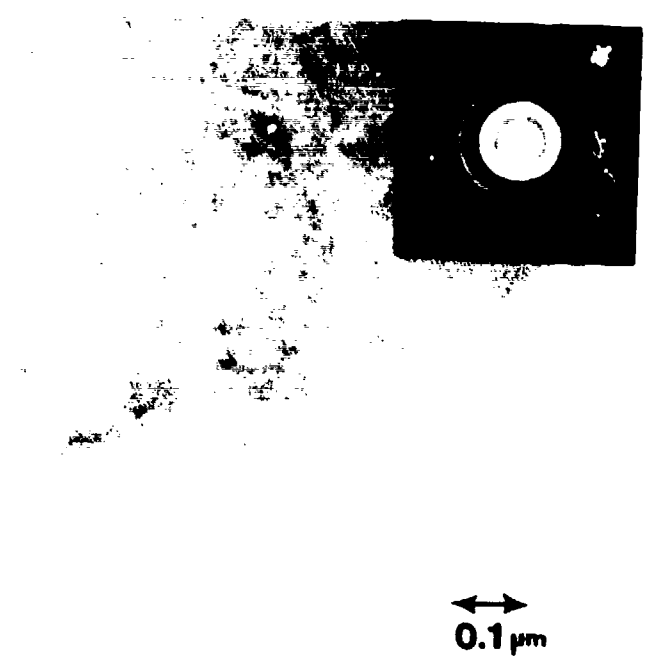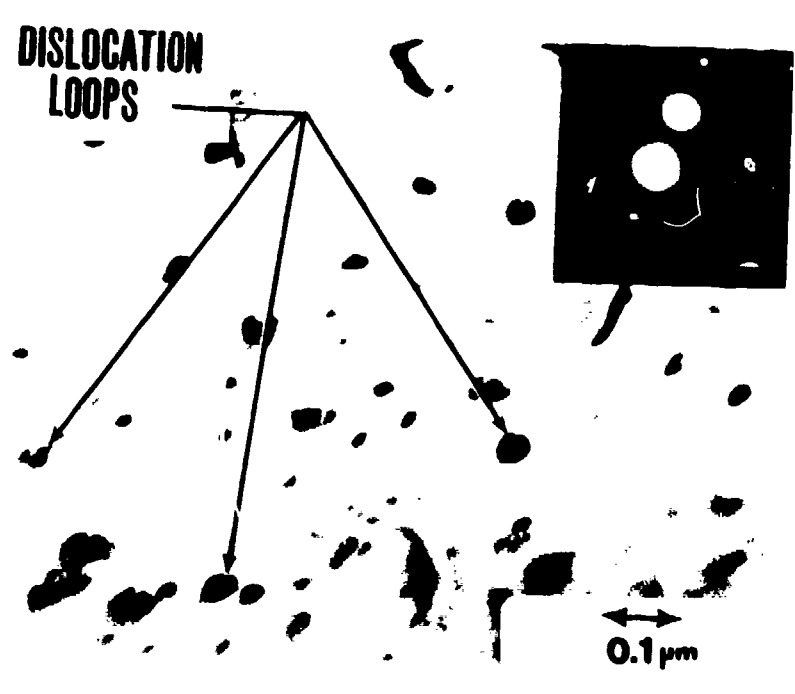
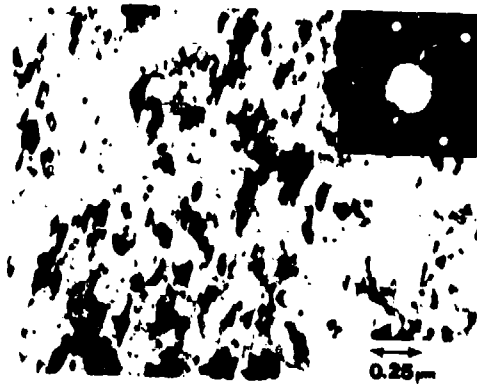ENERGY (MeV)

0.1 μm

(a)

DISLOCATION
LOOPS

0.1 μm

(b)

(a)

(b)

Thermal diffusion of tin in GaAs from a spin-on SnO₂/SiO₂ source

Y. I. Nissim and J. F. Gibbons
Stanford Electronics Laboratories, Stanford, California 94305

C. A. Evans, Jr., V. R. Deline, and J. C. Norberg
Charles Evans and Associates, San Mateo, California 94402

The thermal diffusion of Sn in GaAs from a spin-on SnO_2/SiO_2 source is described. The processing steps leading to reproducible electrical characteristics are presented. Electrical measurements, secondary-ion mass spectroscopy, and Rutherford backscattering analysis have been used to study the diffusion during various processing sequences. The results show that this source can make Sn atoms available for diffusion at very low temperatures and produce heavily doped, shallow n^+ layers that may be of interest for GaAs field-effect transistor technology.

Sn has been used frequently as an n-type dopant in GaAs. The introduction of Sn in GaAs from Sn-doped silicon dioxide has also been reported.[1-3] Recently a new source consisting of a spin-on SnO_2/SiO_2 film was described.[4,5] We are presenting here a study of the thermal diffusion from this source, which shows significantly different chemical and electrical behavior of Sn compared to the doped silicon dioxide sources.

The sample processing steps were as follows. A semi-insulating chrome-doped GaAs substrate oriented along the ⟨100⟩ direction was used. The spin-on source is a tin silica film obtained from Emulsitone,[6] consisting of a mixture of SnO_2, SiO_2, and ethyl alcohol. The film is deposited using a photoresist spinner. A rotation speed of 3000 rpm was chosen, producing a film about 0.3 μm thick. A thermal treatment at 200 °C for 15 min removes the binder (ethyl alcohol) and leaves a layer of SnO_2/SiO_2 with a molecular concentration of about 1:10, according to the vendor. As an encapsulant, a film of undoped SiO_2 (Silox) was deposited on the SnO_2/SiO_2 film. The temperature of deposition was 450 °C. The thickness of this encapsulant is critical to avoid thermal stresses during the subsequent thermal treatments. The oxide thickness should be no more than 0.8 μm. We have chosen 0.5 μm as our standard condition.

Any abrupt changes in temperature will produce stresses that cause the films to peel. For this reason a slow thermal ramp is required before any subsequent thermal treatment. A total time of 15 min with a 50 °C increase per

TABLE I. Ramping cycle only.

T_{ramp} (°C)	ρ ($\Omega/\square$)	μ_H (cm²/V sec)	N_D (atoms/cm²)
750	...	...	...
800	974	1353	4.73×10^{12}
850	224	2255	1.24×10^{13}
900	122	2098	2.44×10^{13}
950	64	2234	4.38×10^{13}

FIG. 1. Van der Pauw stripping and SIMS profile for a sample ramped to 900 °C.

Annealing condition	ρ (Ω/□)	μ_H (cm^2/V sec)	N_D (atoms/cm^2)
15 min ramp +30 min at 700 °C	4667	767	1.75×10^{12}
15 min ramp +45 min at 800 °C	151	1794	2.31×10^{13}
15 min ramp +45 min at 900 °C	20	1750	1.82×10^{14}

GaAs, the duration of the ramp (15 min) is not sufficient for a deep diffusion in the GaAs substrate

Figure 1 also shows mobilities obtained by the differential Van der Pauw measurements, along with the Sze and Irvin mobility corresponding to the measured carrier concentration. One can see that the agreement between the two values is excellent when the concentration of Sn is comparable to the electrically active concentration of Sn. We can see that beyond a depth of about 1250 Å most of the Sn impurities are electrically active and that the measured mobility follows the expected value.

Following the initial ramp, further thermal diffusion was studied. With the SnO_2/SiO_2; SiO_2 "source cap" on the substrate, an anneal was carried out in N_2 ambient after the initial ramp. The temperature of the annealing was the one reached during the ramping cycle. Electrical activity was first detected after a ramp to 700 °C, followed by an anneal at 700 °C for 30 min. Table II summarizes this process where three annealing conditions have been chosen. The sheet carrier concentration varies from 1.75×10^{12} (30 min at 700 °C) to 1.82×10^{14}/cm^2 (45 min at 900 °C). Rutherford backscattering analysis was done on a sample ramped to 900 °C and annealed 5 min at 900 °C. The total concentration of Sn was found to be 6×10^{15}/cm^2. This result suggests that the source cap introduces enough Sn atoms in interstitial sites during the ramping cycle which are then ready for further diffusion and activation.

In light of this last result, we carried out an anneal after removing the source cap. The ramping cycle was done for a range of temperatures varying from 600 to 950 °C. The duration of this cycle was kept constant at 15 min. The source cap was then removed by a 45-sec dip in HF to remove the oxides

minute for the last 8 min was chosen to ramp the samples to the desired temperature. This ramp was carried out in a N_2 ambient.

A Van der Pauw technique was used to measure sheet resistivity, mobility and carrier concentration after the ramping cycle, with the results indicated in Table I. We see from the data that the ramping sequence is responsible for diffusion and electrical activation of Sn. Measurable activity starts at 800 °C with an active dose of 4.73×10^{12} and can reach 4.38×10^{13} atoms/cm^2 at 950 °C.

A comparison of the chemical profile and the electrically active one was obtained from using secondary-ion mass spectroscopy (SIMS) and differential Van der Pauw techniques. The measurements were carried out on a sample ramped at 900 °C and are presented in Fig. 1. It can be seen that only 3% of the total sheet concentration of Sn (7×10^{14}/cm^2) is electrically active. The total diffusion depth is 2000 Å, with most of the Sn atoms located within the first 1000 Å. This was expected in view of the nature of this thermal treatment. Although the temperature of 900 °C is enough to introduce Sn atoms from the source into the

TABLE III: Thermal annealing without source cap.

| Annealing conditions	T_{ramp} (°C)	600	650	700	750	800	850	900	950
30 min at 800 °C	ρ (Ω/□)	521	206	170	89	81	72	54	44
	μ_H (cm^2/V sec)	2747	2633	2285	2169	2110	2254	2283	2079
	$N_D \times 10^{13}$/cm^2	0.436	1.15	1.61	3.22	3.65	3.85	5.05	6.85
30 min at 850 °C	ρ	84	74	54	43	43	40	32	26
	μ_H	2667	2154	2325	2196	2214	2110	2256	2206
	$N_D \times 10^{13}$	2.8	3.9	4.98	6.55	6.64	7.35	8.77	11.1
30 min at 900 °C	ρ	60	43	40	31	28	27	28	22
	μ_H	2353	2341	2381	2199	2111	2103	2098	2176
	$N_D \times 10^{13}$	4.42	6.15	6.63	9.29	10.5	10.9	10.5	13.2
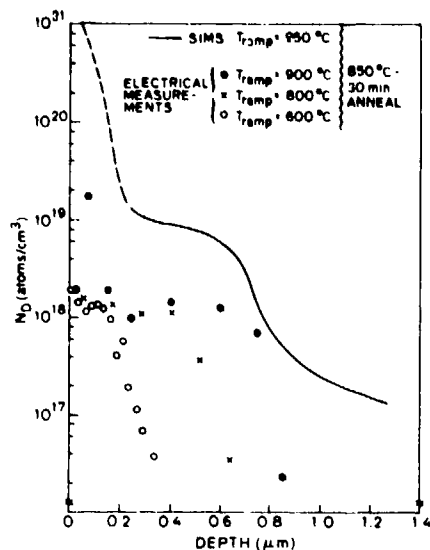
FIG. 2. Van der Pauw stripping result for ramping cycles to 900, 800, and 600 °C followed by an anneal at 850 °C for 30 min with no source cap. Also a SIMS profile for the same sequence with a ramping temperature of 950 °C.

and a 5-min dip in boiling HCl to remove any metallic tin. All the samples were then encapsulated with a film of heavily As-doped SiO_2. Three different sets of samples were annealed for 30 min at 800, 850, and 900 °C in H_2 ambient. Sheet electrical measurements were carried out with the results shown in Table III. A monotonic evolution of the carrier density and sheet resistivity leading to an ultimate saturation for the high-temperature ramping and annealing cycles is obtained. It is interesting to note that Sn can be introduced into GaAs at very low ramping temperatures. This conclusion follows from Table III since no electrical activity was observed after the ramp (Table I).

We focused our attention on the 850 °C anneal for profiling measurements: SIMS analysis was performed on the sample ramped to 950 °C, and differential Van der Pauw measurements were carried out on the samples ramped to

900, 800, and 600 °C. These results are presented in Fig. 2. We can see that the peak of very high Sn concentration is still present after the anneal and that it now spreads to a depth of 3000 Å followed by a flat distribution (SIMS analysis). The active carrier concentration curve also shows a peak near the surface. During the SIMS analysis we have also followed the behavior of oxygen. The wafer studied (ramp to 950/850 °C anneal) reveals that oxygen has been introduced to a depth corresponding to the high peak Sn concentration. Consequently the yield of Sn in this matrix does not correspond to the scale shown in Fig. 2, since the SIMS calibration was performed for Sn in GaAs. This last observation is supported by a Rutherford backscattering analysis showing a lower total concentration of Sn than the SIMS analysis.

As a result of these experiments, we believe that an interface reaction between the source and the substrate occurs. This reaction occurs at temperatures as low as 450 °C and is responsible for a high Sn concentration at the surface. The majority of the Sn is not electrically active until a further anneal.

This source can produce a shallow n^+ layer on an insulating substrate with excellent electrical properties and a high percentage of active dopants below the peak Sn concentration at the surface. These characteristics make this doping source attractive for use in GaAs field-effect transistor technology.

[1]W. van Munch, IBM J. Res. Dev. 10, 438 (1966).
[2]C. F. Gibbon and D. R. Ketchow, J. Electrochem. Soc. 118, 915 (1971).
[3]H Yamazaki, Y Kawasaki, M. Fujimoto, and K. Kudo, Jpn. J. Appl. Phys. 14, 717 (1975).
[4]In. Arnold, H. Dambkes, and K. Heimy, in Digest of Technical Papers, 11th International Conference on Solid State Devices, Tokyo, 1979, p. 89.
[5]J. F. Gibbons, A. Lietoila, Y. I. Nissim, and F. C. Wu, in Proceedings of the 1979 Materials Research Society Symposium on Laser and Electron Beam Processing of Materials (unpublished).
[6]Emulsitone Co., 19 Leslie Court, Whippany, N.J.

cw laser assisted diffusion and activation of tin in GaAs from a SnO₂/SiO₂ source

Y. I. Nissim and J. F. Gibbons

Stanford Electronics Laboratories, Stanford, California 94305

T. J. Magee and R. Ormond

Advanced Research and Applications Corporation, Sunnyvale, California 94086

A new technique for doping GaAs with Sn from a spin-on SnO₂/SiO₂ source is described. Sn is first introduced in the GaAs substrate by a slow thermal ramp. Subsequent diffusion and activation of Sn is accomplished with a cw scanning laser. Results for laser power below and above the melting power of the substrate are presented. Transmission electron microscopy and electron diffraction patterns indicate that a chemical reaction involving the formation of a tin-arsenide compound occurs during the diffusion process.

PACS numbers: 61.70.Tm

The diffusion of impurities in a semiconductor substrate from a deposited dopant source film has been studied for many years. Recently, the use of a SnO₂/SiO₂ source to diffuse Sn impurities in GaAs substrates has been introduced[1-3] and found to have properties of interest for GaAs technology. Experiments by the present authors have used a double "source-cap" layer consisting of a 0.3-μm spin-on SnO₂/SiO₂ film covered by a 0.5-μm film of SiO₂ prepared by chemical vapor deposition. The substrates were ⟨100⟩ Cr-doped semi-insulating GaAs. The description of the processing steps and the behavior of Sn during thermal diffusion are presented in Ref. 3. In this paper we present data illustrating the use of a cw scanning laser to assist the Sn diffusion process that was initiated thermally.

To prevent the peeling of the double-layer source cap during laser irradiation, a slow thermal ramp was carried out in N₂ ambient. Typical thermal pretreatment for optimum laser action is a ramp from room temperature to 900 °C in 15 min. This step apparently breaks down an interfacial barrier to start the diffusion process. So far we have been unable to start the diffusion by the scanning laser alone.

The thermal ramp gives an electrically active Sn concentration of $2-3 \times 10^{18}$ atoms/cm³ to a depth of about 1600 Å in the GaAs substrate. Following this ramp, the wafers were laser treated using the scanning cw argon ion laser system described by Gat and Gibbons.[4] The beam was focused by a 136-mm lens, leading to a 50-μm beam diameter at the focal plane. The spot was then scanned with 15-μm spacing between adjacent lines at a speed of 12 cm/sec. In order to reduce the thermal stress created by the incident beam at the surface of the wafer, the substrate was held during irradiation at 350 °C. These parameters were found to be optimum and were kept constant. The investigation of the different temperature regimes was accomplished by changing only the incident power level. The reflectivity of the substrate with its double-layer source cap was directly measured to be 24%. Using calculations and curves of laser-induced temperatures in GaAs[5] and the above parameters, a maximum surface temperature was associated with each incident laser power.

The diffusion of tin was first studied in a regime where the laser power was kept below the level required to melt the substrate. The laser power for this condition was determined by observing the laser power required to just produce visible thermal etching and then reducing the settings by 5%. A power level of $P = 0.61$ W, leading to a maximum induced temperature of about 800 °C, was obtained. A series of one, three, and five scan frames were performed with the double-layer source cap remaining on the substrate. A Van der Pauw technique was used to characterize the resulting sheet resistivity, Hall mobility, and sheet carrier concentration. The results are summarized in Table I. The increase of the sheet carrier concentration from 2.44 to 3.01×10^{13} cm⁻², accompanied by a decrease of sheet resistivity with a larger number of scans, illustrates either the diffusion from the source and/or the activation of tin impurities introduced during the thermal cycle.

SIMS (secondary ion mass spectroscopy) analysis was performed on a sample thermally ramped only and on a sample scanned five times after the ramping. The profiles show an increase in Sn concentration and an in-diffusion of about 150 Å. To investigate the contribution of the irradiation to the diffusion from the source cap, compared to the activation of the impurity sitting in the substrate after the ramp, the source was removed before the laser scannings. The reflectivity of the bare substrate (after the thermal ramp) was measured and the incident laser power adjusted to reach the

TABLE I. Sheet electrical measurement of the Sn-diffused layer induced by repetitive laser scans.

	ρ (Ω/□)	μ_H (cm²/V sec)	N_s (cm⁻²)
Thermal ramp to 900 °C in 15 min	122	2098	2.44×10^{13}
1 scan with source cap	118	2017	2.63×10^{13}
3 scans with source cap	117	1838	2.91×10^{13}
5 scans with source cap	107	1940	3.01×10^{13}
5 scans with *no* source cap	118	2057	2.57×10^{13}

same maximum temperature ($\simeq 800$ °C) as before. The wafer was scanned five times and the sheet electrical measurements presented in Table I were carried out. The results, when compared with those obtained with the source cap on, suggest that the total increase in active impurities due to laser irradiation is 77% from the source and 23% from the activation of Sn introduced during the ramp.

The action of the laser is found to be more significant if the sample is left "at temperature" for a short time after the ramp. For this reason the above experiment was repeated after thermally ramping the substrate and its source to 900 °C and leaving it for 5 min longer at 900 °C. A series of five scans, inducing a maximum temperature of about 800 °C, was then performed. A differential Van der Pauw technique was used to profile these samples. Figure 1 shows the results obtained before and after the irradiation. A net increase in carrier concentration to a value of about 8×10^{18} cm^{-3} is observed after the scans. The etching rate of these layers was very nonuniform. For this reason the profiles in Fig. 1 should be averaged to a flat distribution ending rapidly at a depth of 2500 Å. The total Sn profile was also obtained using a Rutherford backscattering (RBS) system. A 2.2-MeV incident helium beam incident on the GaAs substrate was used after removal of the source. The spectra obtained in a random orientation from the backscattered particles are presented in Fig. 2. A sample having received a thermal treatment only, another one receiving additional laser scans leading to $T_{max} \simeq 800$ °C, and a third one scanned at higher laser power leading to $T_{max} \simeq 850$ °C were analyzed. The Sn profile is characterized by a large peak concentration at the surface which increased after laser scanning, probably showing Sn diffusing from the source. An increase in the width of the profile after irradiation is also observed. This illustrates the diffusion of Sn in GaAs.

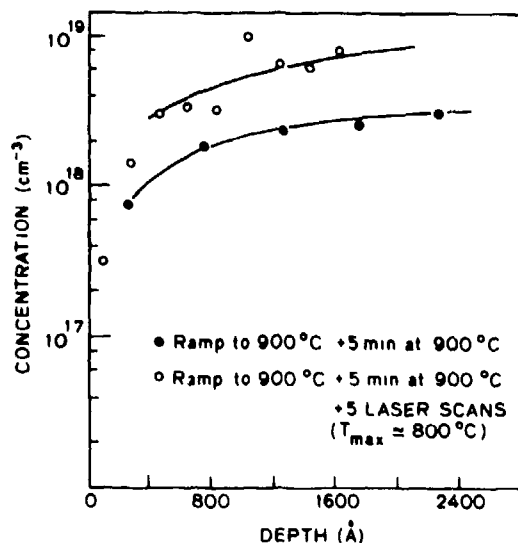Both the RBS profiles and those obtained using SIMS analysis[3] show an anomalously high concentration of Sn close to the surface. No high surface concentration is observed in the electrical profile (Fig. 1). This suggests that a chemical reaction takes place in addition to the diffusion process. To study this possibility, a sample ramped to 900 °C and a sample ramped and scanned five times at a power inducing a temperature of 800 °C were prepared for transmission electron microscopy (TEM) and diffraction analysis using conventional jet thinning techniques. Bright field (Fig. 3) and dark field transmission electron micrographs indicated precipitation after thermal ramp and after laser processing. Selected area electron diffraction patterns revealed that the precipitates were composed of a tin-arsenic compound Sn_3As_2. Additionally, an amorphous $\beta\ Ga_2O_3$ was detected in the samples. After laser irradiation we observed an increase of the amount of surface coverage by $\beta\ Ga_2O_3$ crystallites. In all cases the surface oxide film appeared as a laterally discontinuous film.

FIG. 2. RBS random spectra showing Ga and As edges and the Sn profile.

FIG. 1. Electrical profiles for Sn obtained using a differential Van der Pauw technique.

FIG. 3. Bright field transmission electron micrograph showing formation of As_2Sn_3 plates. In the upper-right-hand corner are the rings associated with $\beta\ Ga_2O_3$ and As_2Sn_3. The d values were measured and checked to be consistent with above compounds.

TABLE II. Electrical measurements of tin-diffused layer induced by the laser at $P \simeq P_{melt} = 1$ W.

Temperature of the ramp	ρ ($\Omega/\square$)	μ (cm^2/V sec)]	μ_H (cm^{-2})	N, (cm^{-2})
700 °C +	0 scans	...	...	...
	1 scan	...	...	...
	2 perpendicular scans	127	220	2.27×10^{14}
800 °C +	0 scans	537	2150	5.45×10^{12}
	1 scan	120	600	8.62×10^{13}
	2 perpendicular scans	54	500	2.36×10^{14}
900 °C +	1 scans	82	2100	3.6×10^{13}
	1 scan	48	850	1.54×10^{14}
	2 perpendicular scans	28	800	2.82×10^{14}

The temperature regime where the incident power is above the melting threshold of the GaAs substrate has also been investigated. Melting occurs at about $P = 1$ W. Different scans were tried in the range 1–2 W. A difference in color observed in the scanned lines as a function of incident power suggests that different tin-arsenide compounds are formed (similar to the silicon-metal reactions[6]). Unfortunately it was impossible to identify these compounds because the substrate cracks during an overlapping scan (for $P > 1.4$ W). The electrical conduction was observed to be significantly better along the direction of the scan compared to a direction perpendicular to the scan. For this reason the wafers were scanned in two perpendicular directions. Table II summarizes the sheet electrical measurements done on samples scanned at $P \simeq P_{melt} = 1$ W with different ramping temperatures. It should be observed that the change in sheet carrier concentration is drastic, but the overall mobilities are low, probably owing to stress lines induced by the laser.

We have shown that a cw laser could assist the diffusion and activation of Sn in GaAs. The small increase in the diffu-sion depth after laser scanning, as compared to a regular thermal diffusion, allowed us to produce shallow n^+ layers, making this new technique attractive for the GaAs technology.

[1]N. Arnold, H. Daembkes, and K. Heime, J. Appl. Phys. 19, 361 (1980).
[2]J. F. Gibbons, A. Lietoila, Y. I. Nissim, and F. C. Wu, in *Laser and Electron Beam Processing of Material*, edited by C. W. White and P. S. Peercy (Academic, New York, 1980), p. 593.
[3]Y. I. Nissim, J. F. Gibbons, C. A. Evans, Jr., V. R. Deline, and J. C. Norberg, Appl. Phys. Lett. 37, 90 (1980).
[4]A. Gat and J. F. Gibbons, Appl. Phys. Lett. 32, 142 (1978).
[5]Y. I. Nissim, A. Lietoila, R. B. Gold, and J. F. Gibbons, J. Appl. Phys. 51, 274 (1980).
[6]T. Shibata, T. W. Sigmon, and J. F. Gibbons, in *Laser and Electron Beam Processing of Materials*, edited by C. W. White and P. S. Peercy (Academic, New York, 1980), p. 530.

Nonalloyed Ohmic Contacts to n-GaAs by CW Laser-Assisted Diffusion From a SnO₂/SiO₂ Source

Y. I. NISSIM, J. F. GIBBONS, AND R. B. GOLD

Abstract—Nonalloyed ohmic contacts were formed on diffused n^+ layers in GaAs. These layers were obtained in semi-insulating substrates by a combination of themal and CW laser-assisted diffustion and activation of tin from a spin-on SnO₂/SiO₂ film. These contacts display low specific contact resistance ($\lesssim 1 \times 10^{-6}$ $\Omega \cdot cm^2$) and good thermal stability (up to 400°C).

The quality of ohmic contacts plays an important role in the performance and reliability of GaAs devices such as the field-effect transistor. Traditional Au–Ge alloyed contacts have a relatively low specific contact resistance (in the low 10^{-6} $\Omega \cdot cm^2$ range) but leave room for improvement in both morphology and thermal stability [1], [2]. In an attempt to solve these difficulties, new techniques have been recently developed for the formation on nonalloyed contacts. For this purpose, molecular beam epitaxy [3], [4] and pulse beam annealing of high ion implanted doses [5] have been used to produce heavily doped n^+ layers. In this presentation we introduce a new diffusion technique to obtain nonalloyed contacts to GaAs.

The n^+ layers are obtained from the diffusion of tin in Cr doped (100) GaAs substrates. The diffusion source is a spin-on SnO₂/SiO₂ film (0.5 μm) encapsulated with SiO₂ (0.5 μm) deposited by chemical vapor deposition. Details of the pro-
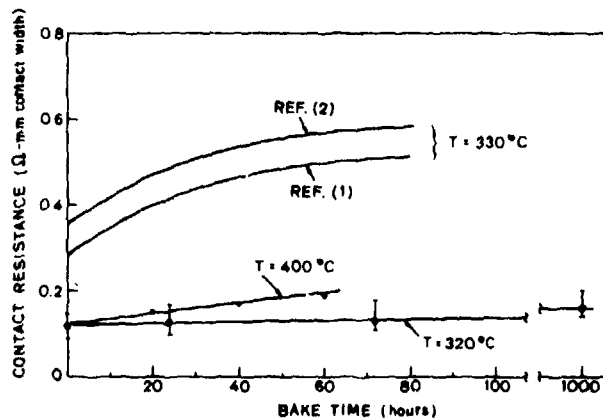
Fig. 3. High temperature stability of planar nonalloyed contacts.

contact width, is plotted for two different temperatures (320 and 400°C) in Fig. 3. 1000 h at 320°C produces an increase in resistance of less than 50 percent. Even at 400°C, the slope of the increase is still small. Published data for the degradation of Au–Ge alloyed contacts are presented for comparison.

This low contact resistance and thermal stability make Sn diffusion from doped films an attractive technique for the fabrication of nonalloyed contacts. The straightforward processing sequence and the broad laser irradiation window suggest a number of applications to GaAs devices.

ACKNOWLEDGMENT

REFERENCES

[1] A. Christou and K. Sleger, "Precipitation and solid phase formation in Au (Ag)/Ge based ohmic contacts for GaAs FETs," in *Proc. 6th Biennial Cornell Elec. Engr. Conf.*, p. 169, 1977.

[2] H. M. Macksey, "Ohmic contacts for GaAs power FETs," in *Gallium Arsenide and Related Compounds 1976*. St. Louis MO:, Inst. Phys. Conf. Ser. 33b, p. 254.

[3] P. A. Barnes and A. Y. Cho, "Non-alloyed ohmic contacts to n-GaAs by molecular beam epitaxy," *Appl Phys. Lett.*, vol. 33, p. 651, 1978.

[4] R. Stall, C. E. C. Wood, K. Board, and L. F. Eastman, "Ultra low resistance ohmic contacts to n-GaAs," *Electron Lett.*, vol. 15, p. 800, 1979.

[5] P. A. Pianetta, C. A. Stolte, and J. L. Hansen, "Non-alloyed ohmic contacts to electron-beam-annealed Se-ion-implanted GaAs," *Appl. Phys. Lett.*, vol. 36, p. 597, 1980.

[6] Y. I. Nissim, J. F. Gibbons, C. A. Evans, Jr., V. R. Deline, and J. C. Norberg, "Thermal diffusion of tin in GaAs from a spin-on SnO_2/SiO_2 source," *Appl. Phys. Lett.*, vol. 37, p. 89, 1980.

[7] S. M. Sze, *Physics of Semiconductor Devices*. New York: Wiley, 1969, p. 38.

[8] Y. I. Nissim, J. F. Gibbons, T. J. Magee, and R. Ormond, "CW laser-assisted diffusion and activation of tin in GaAs from a SnO_2/SiO_2 source," to be published in J. Appl. Phys.

[9] Y. I. Nissim, A. Lietoila, R. B. Gold, and J. F. Gibbons, "Temperature distributions produced in semiconductors by a scanning elliptical or circular CW laser beam," *J. Appl. Phys.*, vol. 51, p. 274, 1980.

CW LASER-ASSISTED DIFFUSION OF TIN IN GaAs FOR NON-ALLOYED OHMIC CONTACTS

Y. I. Nissim and J. F. Gibbons
Stanford Electronics Laboratories, Stanford, CA   94305

R. B. Gold and D. M. Dobkin
Watkins-Johnson Company, Palo Alto, CA   94304

The diffusion of tin in semi-insulating GaAs from a SnO_2/SiO_2 film has been studied [1]. Such diffusion leads to the formation of a thin n^+ layer ($n \geq 10^{19}$ cm^{-3}). We have found that the evaporation of Ti-Pt-Au or Al on these diffused layers produces low-resistance ohmic contacts without requiring a subsequent alloy. This process is of particular interest for GaAs MESFET's since these metallizations are also suitable for Schottky barrier gates on lightly-doped material.

The "source-cap" for the tin diffusion consists of a SnO_2/SiO_2 film (typically 0.3 μm thick and deposited by a spin-on technique), covered by a 0.5 μm film of CVD SiO_2. Single-layer CVD SnO_2 sources and multi-layer CVD SnO_2/SiO_2 sources have also been investigated. The diffusion is initiated by a slow thermal ramp (typically room temperature to 900°C in 15 minutes) after which the wafers are irra-diated with a scanning cw argon laser. A typical incident laser power of 0.6 W is focussed on a 50 μm diameter spot, producing a maximum surface temperature of ~800°C. Carrier and impurity distri-butions in the diffused n^+ layers have been analyzed by differential van der Pauw measurements and SIMS depth profiling, respectively. Following the removal of the "source cap", contact metal is evaporated and a transmission-line pattern is used to evaluate sheet resistance and specific contact resistance.

The effect of the laser irradiation on these values is shown in Fig. 1. It can be seen that the sheet resistance of the n^+ layer is relatively unaffected by the laser, for powers below 0.6 W, but that there is a dramatic effect on specific contact resistance (two orders of magnitude lower than with no laser scan). Contact resistances in the low 10^{-6} Ω-cm^2 range can be obtained for a range of incident laser powers from 0.4 to 0.7 W. The resistance of the resulting planar contacts is roughly 0.1 Ω, for a 1 mm contact width. These contacts appear to be thermally stable; 1000 hours at 320°C produces an increase in resistance of less than 50%.

We have also investigated laser processing in the regime where power is increased to the level which causes melting (~1 W). It is

[1]   Y. I. Nissim, J. F. Gibbons, C. A. Evans., Jr., V. R. Deline and
      J. C. Norberg, Appl. Phys. Lett. <u>37</u>, 90 (1980).

observed that GaAs wafers with the double-layer "source cap" can withstand significantly higher laser-induced maximum temperatures than unencapsulated wafers. Sheet resistances below 30 $\Omega/\Box$ have been produced in this regime.
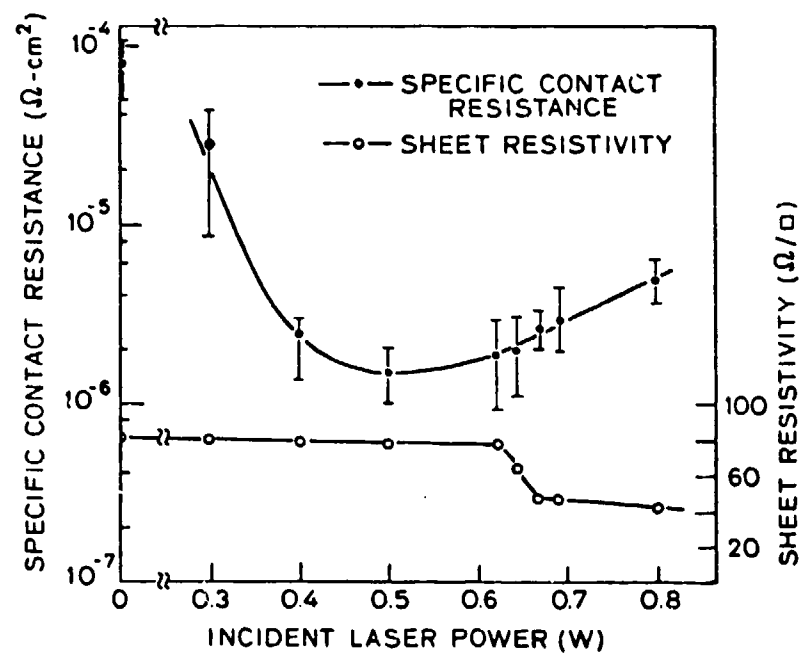
Fig. 1 The effect of laser power on the properties of diffused n^+ layers and non-alloyed Ti-Pt-Au contacts. The bars on the R_{SC} data represent the range of values observed on various runs.